Solar System analogues among exoplanetary systems

Maria Lomaeva

Lund Observatory
Lund University

2016-EXA105

Degree project of 15 higher education credits
June 2016

Supervisor: Piero Ranalli

Lund Observatory
Box 43
SE-221 00 Lund
Sweden

Populärvetenskaplig sammanfattning

Människans intresse för rymden har alltid varit stort. Man har antagit att andra planetsystem, om de existerar, ser ut som vårt: med mindre stenplaneter i banor närmast stjärnan och gas- samt isjättar i de yttre banorna. Idag känner man till drygt 2 000 exoplaneter, d.v.s., planeter som kretsar kring andra stjärnor än solen. Man vet även att vissa av dem saknar motsvarighet i solsystemet, t. ex., heta jupitrar (gasjättar som har migrerat inåt och kretsar väldigt nära stjärnan) och superjordar (stenplaneter större än jorden). Därför blir frågan om hur unikt solsystemet är ännu mer intressant, vilket vi försöker ta reda på i det här projektet.

Det finns olika sätt att detektera exoplaneter på men två av dem har gett flest resultat: transitmetoden och dopplerspektroskopin. Med transitmetoden mäter man minskningen av en stjärnas ljus när en planet passerar framför den. Den metoden passar bäst för stora planeter med små omloppsbanor. Dopplerspektroskopin använder sig av Doppler effekten som innebär att ljuset utsänt från en stjärna verkar blåare respektive rödare när en stjärna förflyttar sig fram och tillbaka från observatören. Denna rörelse avslöjar att det finns en planet som kretsar kring stjärnan och påverkar den med sin gravitation. Dopplerspektroskopin är lämpligast för massiva planeter med små omloppsbanor.

Under projektets gång har vi inte bara letat efter solsystemets motsvarigheter utan även studerat planetsystem som är annorlunda. Vi har hittat tecken på att vissa av heta jupitrar fortfarande kan hålla på och migrera inåt vilket kan leda till att mindre planeter i dessa system blir utkastade.

En annan fråga som dyker upp i detta sammanhang är om det finns liv på andra planeter än jorden. Vi har funnit några kandidater som skulle kunna ha samma uppbyggnad som jorden har. Man kan även definiera gränserna för en så kallad beboelig zon, d.v.s., det avstånd från stjärnan på vilket en planet får lagom med stjärnljus och kan ha vatten i flytande form på sin yta. En planet inom denna zon skulle då, rent teoretiskt, kunna vara bebodd. Bland planeter som vi betraktat fanns det sju sådana. Uppkomsten av ett liv är dock väldigt komplex och beror inte enbart på avstånd från stjärnan. Därför kan man tyvärr inte garantera att det finns ett utomjordiskt liv på dessa planeter.

Solsystemets motsvarigheter är fortfarande väldigt svåra att detektera med dagens teknologier. Därför förblir frågan om deras existens obesvarad. Man behöver uppfinna mer känsliga teleskop som kommer att kunna detektera små stenplaneter samt planeter med stora omloppsbanor. Det återstår att se vad morgondagens upptäckter kommer att visa.

Abstract

Over the past two decades many discoveries of exoplanets have been made, which have drawn much attention to extrasolar planetary systems. In this work we study the composition of these systems and search for analogues of the Solar System.

We considered the planets in the database at exoplanet.eu. The search of solar-like systems required these planets to be classified. The classification was performed using k-means clustering algorithm and planets with measured masses and semi-major axes were divided into three clusters: hot Jupiters, gas giants and the third cluster with rocky and Neptunian planets.

Our first attempt to separate rocky and Neptunian planets by their density was performed by using k-means algorithm for planets with three measured parameters: mass, radius and semi-major axis. The results, however, were not satisfactory and a simple mass limit was chosen instead.

Our examination of the extrasolar systems showed that there are few Solar System analogues. This most probably depends on the selection effects of the present-day detection techniques. Two of them were studied more closely: the Doppler radial velocity and transit technique. The first one is more likely to detect massive planets in close orbits, while the latter is more preferable for planets that pass in front of their host stars and have large radii and short orbital periods. Low-mass Earth-like rocky planets are more likely to be detected by the transit technique. Overall, the distribution of planets in their classes has been shown to follow expectations and selection effects.

The systems that contain hot Jupiters were studied closely and the results suggest that there is a number of hot Jupiters that might likely be caught in the act of migration. Also, the number of transiting extrasolar Neptunes and Earths was compared to the results presented by Petigura et al. (2013). It revealed a discrepancy, which arose due to the correction of the occurrence rate of these planets made by the article's authors.

Rocky planets that potentially can host life were another interesting subject in the search of Solar System analogues. According to our definition of the habitable zone, we found six super-Earths and one Earth-like planet that might be habitable. However, such conclusions need deeper examination of the planetary properties.

Contents

Chapter 1

Introduction

1.1 Planetary Formation

A better understanding of the formation of our Solar System can shed some light onto the formation of other planetary systems by assuming that planet formation occurs in a similar way for all systems. Many theories have been proposed but the solar nebula theory is the most considered today. According to it, a molecular cloud which collapses due to gravitational instability in some of its regions possesses an angular momentum, which prevents it from collapsing directly onto the star. Instead it forms a flat symmetric rotating disk with a centre that coincides with the centre of mass of the system and is located in the plane, perpendicular to the direction of the total angular momentum. It is thought that frictional forces are responsible for this redistribution of material in a cloud: they allow an inward migration of the mass. This leads to a significant loss of angular momentum and enlargement of the radius of the accreting cloud (Perryman 2014).

Massive accretion disks usually appear around stars that are younger than 1 Myr. During this period, gravitational potential energy stored in the gas is converted into thermal radiation due to inward flow of the gas and its accretion onto the star (Pringle 1981, Frank et al. 2002). It evolves further to low mass accretion disks which are typical for stars with ages between 1-10 Myr. At late evolutionary stages, i.e. stars aged older than 10 Myr, secondary disks, or debris disks, are generated by collisions of planetesimals. During this period, accretion has ceased and most of the gas has dissipated from the cloud.

The transition between the protostellar and protoplanetary disk is rather arbitrary and ambiguous. However, the protoplanetary phase can be referred to as the final stage of the evolution of the protostar, i.e., when accretion rate is low and most of the mass in the disk has been used for accretion, the gas is dispersed and formation of planets takes place. Planetary formation processes strongly depend on the lifetime of the pro-

toplanetary disk: the longer the lifetime, the more material that is present to create planets (Perryman 2014).

1.1.1 Formation of Terrestrial Planets

The formation of terrestrial planets begins in the mid-plane of the debris disk where most of the dust grains concentrate in the absence of turbulence. Dust grains are considered to be condensed particles in the interstellar medium with sizes of about 1 μm. Electrostatic forces and collisions between them make them stick together and eventually grow in size and form larger bodies and rocks with sizes up to $\sim$10 m (Kusaka et al. 1970). As they increase in size, their relative velocities will also increase to tens of m/s, which most probably will lead to bouncing and fragmentation of the bodies rather than their growth (Chambers 2014).

Today there are two models that consider turbulence effects and explain how this barrier, also called "metre-size-barrier", can be overcome, which allows planetesimals to form directly from smaller particles. The "streaming instability" states that if there is a sufficient amount of cm-to-m-sized particles in a cloud, a rapid drift and accumulation of these bodies will occur in the nearest local pressure maximum of turbulent regions (Chambers 2014, Righter & O'brien 2011). The "turbulent concentration" model implies that mm-sized particles will experience a drag caused by turbulent eddies and gather in the stagnant regions between them. This will result in formation of gravitationally bound clumps and eventually planetesimals.

Planetesimals are generally defined as solid objects of size $\gtrsim$1 km which are created in connection with planet formation. Their orbital dynamics are almost independent of the gas drag and they are held together mostly due to self-gravity. The latter allows them to retain the material during collisions and to continue to grow further (Chambers 2014). At this stage collisions can cause both growth and fragmentation of the planetesimals depending on their internal strength and relative velocity, which also determines the collision rate (Chambers 2010, Chambers 2014). As planetesimals increase in mass and size, their gravitational field increases as well. Then, collisions due to gravitational interactions become more important, since now the effective cross-section[1] dominates over the physical cross-section of the planetesimals (Perryman 2014).

More massive bodies are shown to grow faster than small ones, a process called runaway growth. Larger bodies usually obtain nearly circular coplanar orbits due to dynamical friction. This increases the probability of colliding. Smaller bodies, on the contrary, tend to have highly eccentric inclined orbits and thus, lower chance of colliding (Cham-

[1] An approximate concept stating that a collision occurs when two objects encounter each other (Molisch & Oehry 1998).

bers 2014). Runaway growth ends when the largest planetesimals have a sufficient mass to control the motion of the smaller bodies in their vicinity. This new regime called oligarchic growth is then established, which means that different regions of the disc are now dominated by one massive body, i.e. a planetary embryo (Chambers 2010).

The gravitational potential of an embryo will perturb the orbits of smaller bodies inside a region called the feeding zone, whose size is proportional to the mass of the embryo. Then accretion of mass will continue due to collisions. When all mass from the feeding zone is used, the maximum mass, or isolation mass, of the embryo is obtained (Chambers 2010). When an embryo reaches the size of the Moon or larger, it can accrete an atmosphere from the gas in the disk. If a planetesimal or a colliding fragment moves through the atmosphere it will experience drag, which gives a higher probability of capturing the body. Thus, the time scale of the oligarchic growth can be substantially reduced due to the presence of an atmosphere (Chambers 2014).

The next stage is the post-oligarchic phase, during which planetary embryos are roughly separated. Their orbits start to cross each other, which leads to an increase in inclination and eccentricity. This perturbs gravitational interactions between the embryos and other material in the disk decreasing the growth rate. This period is also characterised by violent collisions between embryos, which determine the final structure of the system (Perryman 2014). It also depends on other factors, such as initial conditions (O'Brien et al. 2006), the viscosity of the protoplanetary disk (Lin & Papaloizou 1979), planetesimals surface density (Raymond et al. 2005) and presence and migration of giant planets (Levison & Agnor 2003).

1.1.2 Formation of Gaseous Planets

Today there are two theories that explain formation of gaseous planets: the core accretion model and the disk instability model (Perryman 2014, D'Angelo et al. 2010).

The Core Accretion Model

The core accretion model is the most widely used one and can explain formation of gas and ice giants in the Solar System as well as exoplanet giants orbiting their host stars at the distance of 10-50 AU (Perryman 2014). It describes the formation of gas giants as a two-step process. First, accretion of the solid core takes place until the mass of the planetary core exceeds the critical value of $\sim$5-20 $M_\oplus$ (Perryman 2014). At masses of a few Earth masses H and He can be captured into the gaseous envelope around a planet, which is shown in Figure 1.1. This graph shows the strength of the gravitational field required for capture of diverse elements and molecules. The dashed lines show the maximum velocity of the particles, i.e., 10 times the average velocity,

for a range of temperatures.

The simulations have shown that formation of such massive cores can only occur in the outer disk beyond the snow line, i.e., at a certain distance from the host star where the nebular gas condense into ices (Kennedy & Kenyon 2008). At this distance there is a sufficient amount of accretion material which, in combination with the diminished gravitational dominance from the host star, benefits the formation of gas giants (Perryman 2014).

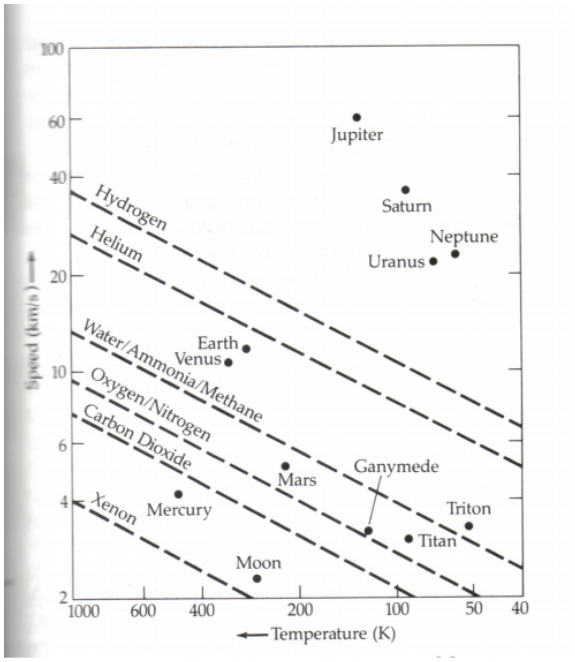

Figure 1.1: Maximum velocities of different elements and molecules. The dots denote the temperature and strength of the gravitational fields of different objects in the Solar System and show what elements they could possibly capture (figure from the lecture notes by prof. Rice at the University of Edinburgh).

Further accretion of material leads to a collapse of the gas envelope because now the pressure gradient cannot resist the gravitational force. The gas becomes rapidly contracted allowing more gas accretion and triggers new contractions. This stage is usually referred to as runaway gas accretion during which the gas is accreted at an ever-increasing rate (D'Angelo et al. 2010).

The runaway gas accretion ceases when the mass of a protoplanet exceeds a few tenths of the mass of Jupiter. Then accretion rate decreases until no more gas can be supplied by the disk. This sets the upper time limit for the formation of gas giants (Gargaud et al. 2011). The termination of the gas supply might depend on the disk gap opening or dissipation of the gas. In any case, a reasonable conclusion might be that the final composition of a system is very sensitive to the initial conditions which determine the time scale of the gas dissipation (Perryman 2014).

Gravitational Disk Instability Model

Another formation mechanism is proposed by the gravitational disk instability model. Here the formation of gas giants resembles the formation of stars and is described as a rapid single-step process. This occurs due to gravitational collapse in a massive unstable protoplanetary disk (Perryman 2014). There is a finite probability that a

protoplanetary disk will experience some gravitational instabilities, which will cause its fragmentation into bound, self-gravitating clumps (D'Angelo et al. 2010).

According to this model protoplanets accrete most of the gas already at early stages while the disk is still massive (Perryman 2014) and have more time to accrete heavy elements and planetesimals onto the core. Gravitational instabilities are more likely to occur in the outer regions of protoplanetary disks, which is in agreement with the presence of high-mass planets in outer orbits in both the Solar System and other systems as well (D'Angelo et al. 2010).

There are, however, some serious disadvantages with this theory. First of all, it is unclear how planets that are formed at such early stages evolve with time (D'Angelo et al. 2010). It can neither explain why Solar System giants have similarly large core masses (Perryman 2014) nor the correlation between the stellar metallicity and formation of gas giants (Kikuchi et al. 2014), which is explained by the core accretion model (e.g., Ida & Lin 2004). Furthermore, it has been shown by Kratter et al. (2010) that planetary-mass clumps formed due to disk instability would form brown-dwarfs and M-star companions.

1.2 Planetary Migration

1.2.1 Type I and Type II Migration Regimes

The question about planetary migration became interesting after the discovery of the first hot Jupiter in 1995. Before that there were theoretical studies of planetary migration, primarily of the Solar System planets, suggesting migration of Jupiter at both its early and late stages of formation. However, its final position remained beyond the snow line, where formation of gas giants occurs according to present-day theories. Thus, one of conclusions was that migration did not affect Jupiter significantly, which also was thought to be true for other planets (Lubow & Ida 2010).

During later stages of planetary formation, the gas in the disk is not yet completely dispersed. Then interactions between a young planet and the surrounding disk are possible, which will alter the orbital energy and angular momentum of the planet (Lubow & Ida 2010). As the planet moves through the gas disk, it will excite spiral density waves within the disk (Perryman 2014). This disturbances in the disk will act back at the planet and exert a net torque on it. It will result in a radial motion of the planet through the disk, i.e., migration of the planet (Lubow & Ida 2010).

Planets with masses in the range 1-10 $M_\oplus$ will not affect the density profile of the disk significantly. Migration of such planets due to the exerted net torque is referred to

as the Type I migration regime. The time scale of this regime varies inversely with planetary mass, thus, more massive planets migrate faster (Lubow & Ida 2010).

The Type I regime ends for planets that have become more massive than 10 $M_{\oplus}$, since now they are massive enough to modify the density structure of the disk. Migration of such planets is explained by the Type II regime. At this stage, the angular momentum of the planet can dominate the viscous forces of the disk. Thus, the planet will push away the gas in its vicinity and open a gap in the disk around its orbit (Perryman 2014). The disk and the planet still interact gravitationally but now the torque exerted by the disk is reduced due to the gap. Assuming that the mass of the planet is much smaller than the mass of the disk (Lubow & Ida 2010), the planet will follow the motion of the gas flow (inward or outward) while remaining in the gap (Perryman 2014). Under typical disk conditions the mass required for opening of the gap is about a few tenths of the Jupiter mass (Lubow & Ida 2010).

1.2.2 Alternative Migration Models

Type I and Type II regimes mean that migration of a planet occurs due to its loss of orbital energy and angular momentum to the protoplanetary disk. This should result in low orbital inclinations and eccentricities of the planets when migration is completed (Naoz et al. 2011). This is not necessarily true because, according to the observations, there are some hot Jupiters [2] with highly eccentric orbits, which sometimes are also misaligned with the direction of the host star's spin. Possible explanations for high orbital eccentricity have been proposed by several theories, including secular interactions with a binary star (Holman et al. 1997), interactions with a fly-by star (Malmberg et al. 2011) or planetary interactions (Martin & Livio 2015). The retrograde planetary orbit relative to the total angular momentum of the system can be explained by the interactions with another planet or a brown-dwarf which are further away from the host star than the perturbed planet (Naoz et al. 2011).

1.3 Habitable Zone

A distinctive feature of the Solar System is the fact that it harbours life. This makes the search for rocky planets inside the habitable zone [3] (HZ) of a great interest.

Calculations of the HZ require knowledge about several parameters (Traub & Oppenheimer 2010). First, one has to know the fraction of the absorbed incident stellar

[2] Hot Jupiters are short-period gas giants with orbits close to their host stars (Ford 2014). They are thought to have migrated inwards after being formed beyond the snow line (Martin & Livio 2015).

[3] The range of orbital distances from the host star, at which liquid water can be maintained on the surface of a planet (Martin & Livio 2015).

radiation, (1-A_{bond}), where A_{bond} is the Bond albedo, i.e., the ratio between the total reflected light and total incident light from the star. Another required parameter, f, describes the rotation of a planet. For a rapid rotator f=1, while f=0.5 for a slowly rotating or tidally locked planet with no heat transfer from the cold to hot regions. The composition of the planetary atmosphere is also important because it can provide with information about the greenhouse effect of a planet.

If these parameters are unknown, an assumption that terrestrial exoplanets have Earth-like properties is made. Then, the HZ will scale as the square root of the luminosity of the host star, $L_*^{1/2}$. Mass-luminosity relation for solar-like main sequence stars is

$$\left(\frac{L_*}{L_\odot}\right) = \left(\frac{M_*}{M_\odot}\right)^4$$

where $L_\odot$ and $M_\odot$ are the luminosity and mass of the Sun respectively. The HZ in the Solar System is empirically defined to be in the range of distances between 0.7 AU and 1.5 AU. Hence, the HZ for an Earth-like exoplanet, a_{HZ}, can be defined as the range

$$(0.7\text{AU})(M_*/M_\odot)^2 < a_{\text{HZ}} < (1.5\text{AU})(M_*/M_\odot)^2$$

1.4 Database

Properties of currently known exoplanets are provided by a database at exoplanet.eu. This database was established in 1995 and is frequently updated guaranteeing access to trust-worthy information which includes the latest detections and corrections. The data comes from publications or submissions confirmed by professional journalists or pronouncements made by professional astronomers in professional conferences. The data sources are diverse: books, publications, thesis, reports and first-hand updated data on a number of professional websites. The planets in the database were discovered by using different detection techniques and methods, such as Doppler radial velocity, transit, astrometry, microlensing, direct imaging etc.

In order to obtain a definition of a planet the authors of the database proceeded from the formation evolution, i.e. the accretion process in a protoplanetary disk. The physical criteria for exoplanets is the mass limit of 30 Jupiter masses. This particular mass was chosen since it is the minimum mass needed to create a substellar companion (Schneider et al. 2011). They also allowed an uncertainty in the mass value of 1σ, which gives the upper mass limit of the exoplanets of 30 M_{Jup}+1σ.

In the database four categories of exoplanets can be found: confirmed, candidate, retracted and controversial. Confirmed exoplanets were unambiguously claimed in a professional conference or in a paper that has been accepted. Note that unconfirmed, controversial and retracted planets were not included in the exoplanet table and, thus, not considered in this work.

1.5 Detection Techniques

Doppler Technique

Stellar radial velocity is a useful spectroscopic tool which can reveal the presence of a planet orbiting around star. Radial velocity is usually interpreted as the motion of an object along the line of sight and is normally obtained from observed displacement of stellar spectral lines with respect to their position in an inertial reference frame, i.e., the Doppler shift (Lindegren & Dravins 2003). One of the reasons for the Doppler shift in stellar spectra is gravitational interactions caused by an extrasolar planet that orbits its host star. This can provide with information about the most important properties of the planets: planetary orbital period, orbital eccentricity and mass. However, due to the inclination angle, i, one can only measure the minimum planetary mass, $M \sin i$. The amplitude of the radial velocity is proportional to the mass and the orbital distance of the planet. For example, the impact on the radial velocity signal of the Sun made by Jupiter is 12 m s^{-1} with a period of 12 years, while Earth induces a signal of 0.1 m s^{-1} with a period of one year, which is obviously much smaller. Thus, the Doppler detection technique is more suitable for massive planets in closer orbits since they affect the radial component of the stellar velocity the most.

Nevertheless, the radial velocity precision has drastically improved over the past two decades: from 15 m s^{-1} in 1995 by using the CORALIE instrument to 3 m s^{-1} in 1996 by using HIRES and 1 m s^{-1} in 2003 by HARPS. The major consequence of this precision improvement is that the mass of the detected exoplanets has decreased from 3,000 $M_\oplus$ to 1.1 $M_\oplus$ (Mayor et al. 2014).

The detection rate as a function of mass and orbital period for HARPS and CORALIE planets was presented by Mayor et al. (2011), who studied a sample of 155 planets, which belong to 102 planetary systems. The results in Figure 1.2 represent the detection rate for the HARPS subsample. Since HARPS is the most precise present-day radial velocity instrument, this detection rate is the best achieved so far (Mayor et al. 2014).

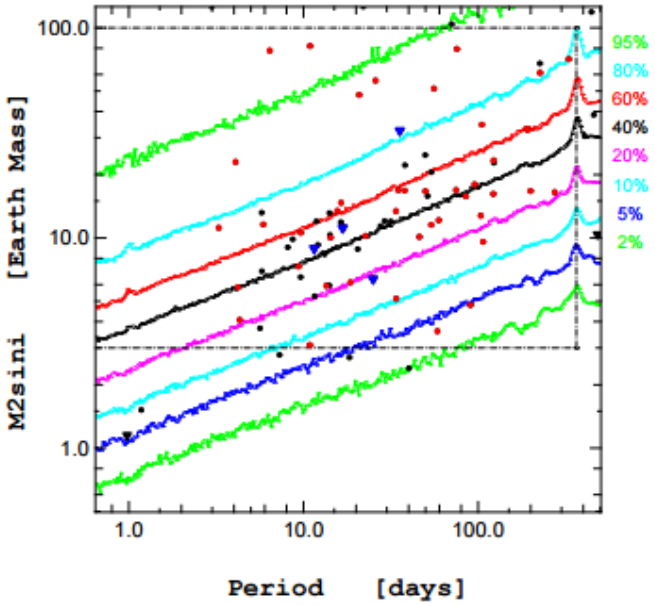

Figure 1.2: Detection probability curves for the HARPS planets (coloured lines). At longer orbital periods a higher mass is needed for detection. The red dots denote the planets, which have been used to correct the detection rate in the region inside the dashed lines. The blue triangles represent planet candidates and have also been used to compute the occurrence rate (figure from Mayor et al. 2011).

At the meter-per-second precision level, one has to correct for other processes that can contribute to the Doppler shift of stellar spectral lines, such as granulation, magnetic features and long-term activity cycles (Mayor et al. 2014). Also, precise measurements require that observations are made in an inertial reference frame. Then the rotation of the Earth around its axis and the barycentre of the Solar System must be taken into account as well (Perryman 2014).

Transit Technique

When a planet passes in front of its host star, a dip in the detected stellar flux will be observed. An example of such an intensity dip is shown in Figure 1.3.

The transit method relates the radii of the planet, R_p, and of the star, R_*, to the decrease of the detected flux, B, as follows:

$$\frac{R_\mathrm{p}^2}{R_*^2} = B$$

Stellar radius and mass can be deduced from the stellar colours, or even better, from stellar spectrum (Lissauer et al. 2014). The semi-major axis of the orbit of the planet a can be calculated from Kepler's 3rd law

$$\frac{P_\mathrm{p}^2}{a^3} = \frac{4\pi^2}{G(M_* + m_\mathrm{p})} \approx \frac{4\pi^2}{GM_*}$$

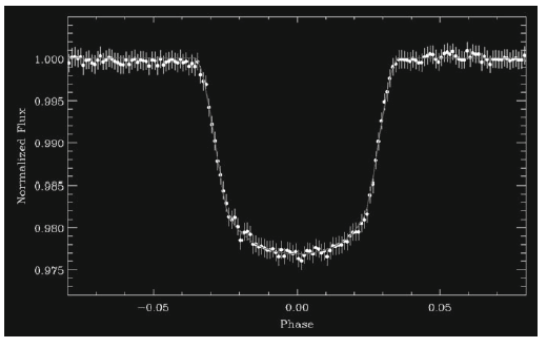

Figure 1.3: A decrease in detected flux of CoRoT-1 as CoRoT-1 b passes in front of it (figure from Kitchin 2012).

where P_p is the period of a planet, G is the gravitational constant, M_* and m_p are stellar and planetary mass respectively.

The selection rules for the transit method resemble those of the Doppler technique: an exoplanet should have a large radius and a short period. Short distance to the star is also desirable since it gives a possibility to observe exoplanets from a larger range of angles as is shown in Figure 1.4.

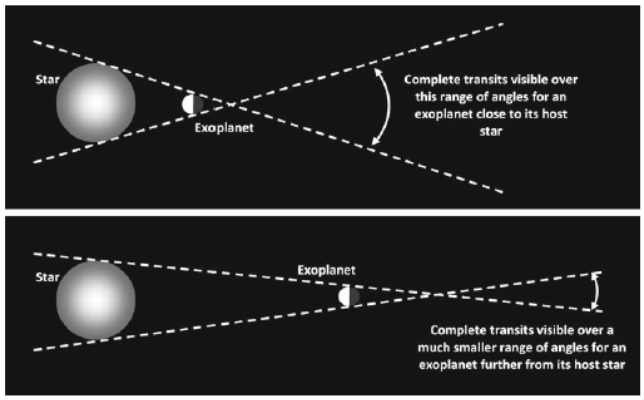

Figure 1.4: An illustration of how the distance between an exoplanet and its host star affects the range of angles at which the transit of the exoplanet can be observed (figure from Kitchin 2012).

The most successful transit mission was carried out by the Kepler space telescope (Winn & Fabrycky 2015). It has monitored around 200,000 stars, of which about 140,000 are dwarf or main-sequence stars (Lissauer et al. 2014). The high precision of the Kepler telescope and absence of atmospheric perturbations have made it possible to detect exoplanets with masses down to $\sim$1 $M_\oplus$ and periods of about one year (Winn & Fabrycky 2015). However, the probability to detect planets with a radius $R_\mathrm{p} \lesssim 2R_\oplus$ and a period of $P_\mathrm{p} \lesssim 200$ days decreases drastically, leading to incompleteness of Kepler catalogue, as is shown in Figure 1.5.

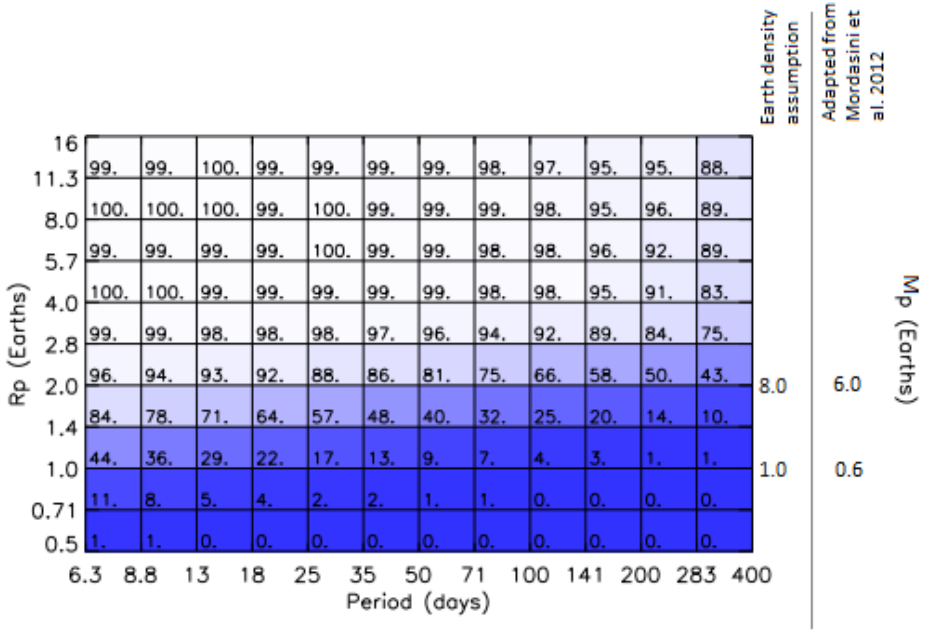

Figure 1.5: Completeness values in Solar76k catalogue (Silburt et al. 2015), which contains planets detected by Kepler. The completeness percentage is denoted by the numbers in the grid cells. High completeness is marked by white colour and low by blue. The vertical scale on the left side denotes planetary radius, while on the right side two scales denote the mass. The mass values to the left were obtained by assuming Earth density for all planets. The values to the right were obtained from Mordasini et al. (2012) for planets having of 50% ice 50% rocky composition (see Section 2.2). The radii of 2 $R_\oplus$ are critical, at which a transition from an occurrence rate of $\sim$100% to values less than 50% occurs. For large orbital periods this value decreases even more (figure modified from Silburt et al. 2015).

The combination of the transit and Doppler methods provides with a very important property of the exoplanets: the density. This property could in principle allow to classify exoplanets, which is essential in the search of Solar System analogues.

Chapter 2

Method

2.1 K-means Clustering

K-means clustering is a simple way of automatically classifying a set of individual data points. Besides the data points, the input in this algorithm is the number of clusters, k, that are going to be generated. The output is a set of centroids, one for each cluster. Also, this method requires an initial guess for the centroid coordinates. Each data point will be assigned as a part of the cluster, which gives the minimum distance between its centroid and the data point.

This will then be followed by a calculation of the average distance between all points in a cluster and the corresponding centroid. This distance is defined as a sum of the square distances between a data point and its nearest centroid. Then the coordinates of the centroid will be changed, such that, it is now located at the centre of the cluster. However, this will mean that the distance between some points and their initial centroids will no longer be the minimal distance, hence, they will be reassigned to a different cluster. Computations will continue until the results converge, i.e., there are no points that change their cluster membership or the coordinates of the clusters do not alter.

This is an efficient and comprehensible method, however, it has some disadvantages. The data must consist of well-separated points, since overlapping data will not be resolved by the algorithm, leading to a lower number of clusters than expected. Also, in some circumstances, this method gives different results for different representation of the same data set. This occurs due to the sensitivity of the method to the initial conditions. However, for our analysis this was a minor effect which did not cause any instability of the routine. In the case of initially well-separated data set as ours, k-means algorithm was the best alternative, being an easy unsupervised clustering algorithm.

2.2 Data Classification

In order to be able to search for Solar System analogues, it is important to have a clear and precise definition of the Solar System. In this work, we chose the mass ordering of the planets in a multi-planetary system to be the crucial criterion for the comparison. This means that eccentricity of planetary orbits was neglected, which however, lowers the precision of the model. Thus, we also chose to classify the exoplanets into four groups: hot Jupiters, gas giants, rocky and Neptunian planets. Decisive factors here were the mass of a planet, its position relative to the host star and even density for rocky and Neptunian planets in the first classification approach.

Exoplanets from the database were loaded and imported into TOPCAT [1], which is a software for viewing and editing tables (Taylor 2005). The main properties of the exoplanets used for classification were the mass and semi-major axis. A few planets with values for semi-major axis larger than 100 AU were removed since they increase noisiness in the cluster classification. Moreover, many of their properties are still not known well enough. The period of such planets is extremely large, preventing a follow-up with radial velocities. For example, 11 Oph b lies 243 AU away from its host star and completes one period in 2,000 years. These planets were detected by direct imaging, hence, their mass is only known after assuming a value for their albedo and density.

K-means clustering [2] was performed in Matlab. To enhance the precision of the exoplanet classification, planets that belong to single-planet systems were considered as well as planets in multi-planetary systems. By visually inspecting the plot that shows planetary mass as a function of semi-major axis, three main groups of planets were expected, as is shown in Figure 2.1. Thus, we chose the input number of clusters to be three.

[1] TOPCAT webpage: `http://www.star.bris.ac.uk/~mbt/topcat/`

[2] The routine is described in this tutorial: `http://www.weizmann.ac.il/midrasha/courses/MatlabIntro/PPT/Lecture_9_-_Unsupervised_Learning_and_Clustering.pdf`.

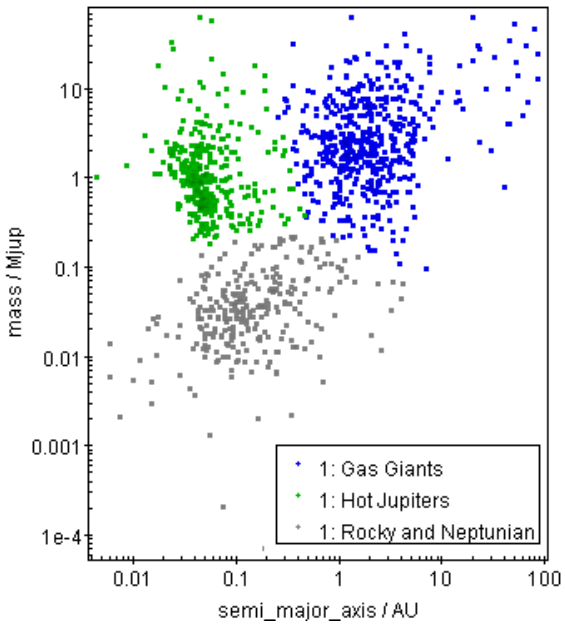

Figure 2.1: Mass vs. semi-major axis for all confirmed planets in exoplanet.eu as of 2015-05-10. Three main groups may be identified. The colours show the result of classification using k-means clustering.

Since a single cluster could be identified for rocky and Neptunian planets together, separation of these planet categories needed special treatment. In this case, only planets that have a measured radius, mass and semi-major axis were considered because the major difference between rocky and Neptunian planets lies in the density. For example, the densities of the Earth and Mars are 5.5 g/cm^3 and 3.9 g/cm^3 respectively, while for Jupiter and Neptune the densities are 1.3 g/cm^3 and 1.6 g/cm^3 respectively (Allen & Cox 1999). K-means algorithm was repeated using only the planets previously classified as rocky or Neptunian and using three variables instead of two. The result was two clusters with one centroid each (see Figure 2.4). Next, we wanted to reduce the 3D classification to a 2D one by only considering mass and semi-major axis, to be able to apply it even to planets without a measured radius. Knowing the coordinates of the centroids, one could make an estimate of the border between the clusters by saying that it goes through the point that is equally distant from the two centroids.
The equation of a linear function $y(x)$ has a form

$$y(x) = kx + m$$

where k is the slope defined as $\frac{\Delta y}{\Delta x}$ and m is a constant. The equation itself was obtained from

$$y - y_1 = k(x - x_1) + m$$

where (x_1, y_1) are coordinates of one of the centroids.

The normal to this line, which also is the cluster border, can be calculated by

$$y - y_q = -\frac{1}{k}(x - x_q)$$

where (x_q, y_q) are coordinates of the middle point.

The resulting line describes mass as a function of semi-major-axis and has an equation $M = -0.67a - 2.35$, where M and a denote mass and semi-major axis respectively. Gas giants and hot Jupiters remained separated in the same manner as in Figure 2.1, while the cluster with rocky and Neptunian planets is separated as shown in Figure 2.2.

A closer look at the density distribution of rocky and Neptunian planets (see Figure 2.3) shows that rocky planets tend to have larger density compared to Neptunian, which is reasonable. Nevertheless, the density dispersion of both planetary types is large and they overlap each other over a wide range of densities.

Cluster separation of rocky and Neptunian planets is shown in Figure 2.4 which is a 2-D projection of a 3-D plot. The exoplanets in this cluster are classified depending on their radius, mass and semi-major axis. The obtained separation shows reasonable results for the Solar System planets.

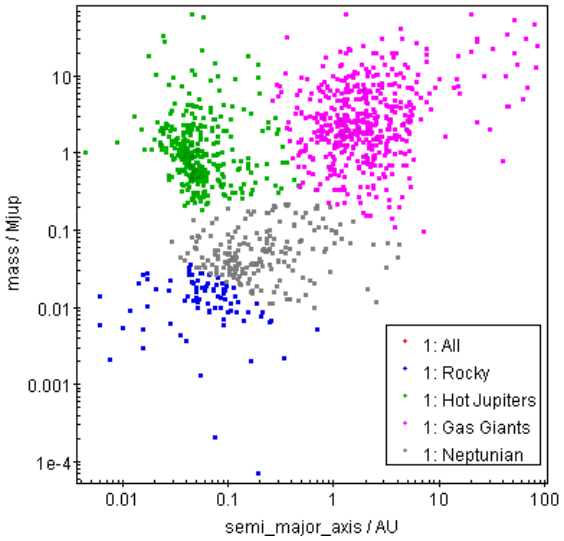

Figure 2.2: Clusters of hot Jupiters, gas giants, rocky and Neptunian planets. The separation of rocky and Neptunian planets depends on both semi-major axis and mass.

This classification method has, however, some disadvantages. The separation of the cluster for rocky and Neptunian planets is not completely satisfactory and the density does not seem to influence the classification. The separation appears to be just a symmetric split of the mass/semi-major axis plane. Also, the requirement of having three known properties (radius, mass and semi-major axis) decreases the number of data points leading to lower precision of the separation. Therefore, the line might shift if the amount of data point increases. Another disadvantage is that the uncertainty of the classification increases when both mass and radius are used because of the addition of the errors in mass and radius.

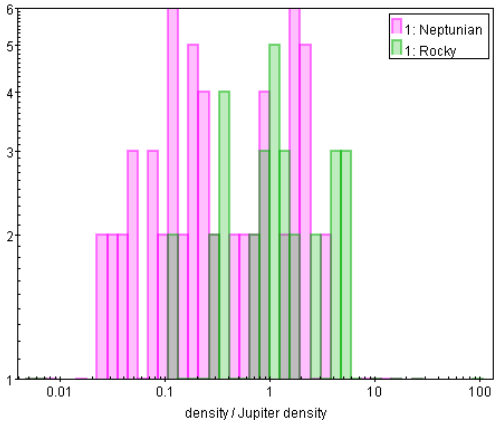

Figure 2.3: Density distribution of Neptunian (magenta) and rocky (green) planets.

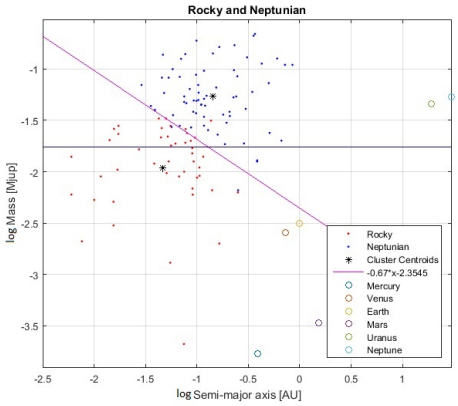

Figure 2.4: Separation between the clusters of rocky and Neptunian planets.

Instead of density, we decided to use planetary mass for the separation. Wolfgang & Lopez (2015) suggest that planets with radii in the range $1.2<R_p<1.8$ $R_\oplus$ can be either rocky or gaseous. We chose to use the conservative definition and opted for the higher limit of this range to be the maximum radius of a rocky planet. By assuming for simplicity that the density is constant and equal to the density of the Earth, the mass becomes proportional to the radius and scales as $M \propto R_p^3$. This gives a mass limit of 5.8 $M_\oplus$ and, hence, the cluster with rocky and Neptunian planets becomes divided by a horizontal line as is shown in Figure 2.5. Now, the density distribution of the rocky planets is less spread out over a lower range of densities (see Figure 2.6). However, there is still no prominent distinction in the density for these planetary types. It may depend on the range of radii between which a planet can either be rocky or Neptunian as it is mentioned above. It may also be a result of errors in mass and radii, which are discussed in Section 2.3.

In a more realistic model, the density of a planet is not constant. Instead, the density gradient becomes steeper for planets with larger masses due to enhanced pressure on the material that a planet consists of because of the gravitational effects (see right panel in Figure 2.7). Mordasini et al. (2012) considered three different scenarios for the mass-radius relationship (see left panel in Figure 2.7) depending on the planetary composition. They distinguished planets that are purely rocky (the red curve) and resemble the composition of the Earth, planets which are 50% ice and 50% rocky (the green curve) and planets which consist of pure ice (the blue curve) and might not exist in nature. For the chosen maximum radius of rocky planets, $R_p = 1.8$ $R_\oplus$, the green curve gives a corresponding mass of about 4 $M_\oplus$, which only differs from the result obtained before by a factor of 1.5. Thus, one could assume that a typical rocky or Neptunian exoplanet consist of equal amount of ice and rock. For more precise mass-density conversion one has to study the composition of each exoplanet separately which

is beyond the scope of this work and hence, was not taken taken into account.

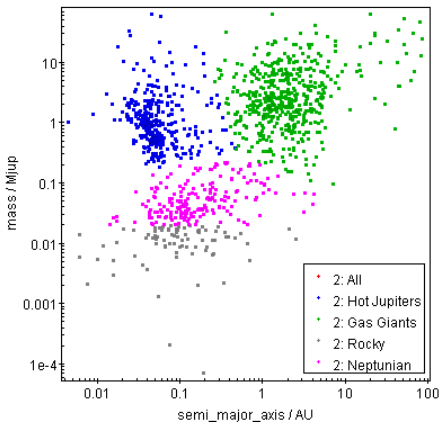

Figure 2.5: Clusters of hot Jupiters, gas giants, rocky and Neptunian planets. The separation of rocky and Neptunian planets depends only on mass.

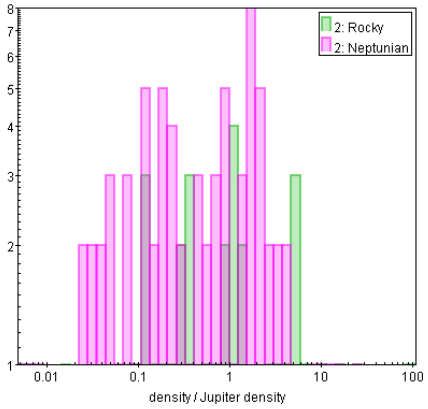

Figure 2.6: Density distribution of rocky and Neptunian planets which were separated by mass only.

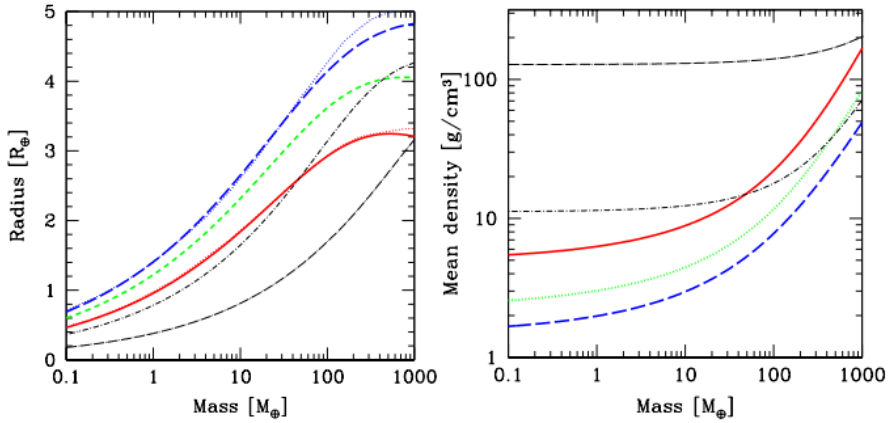

Figure 2.7: Total radius of a planet or planetary core and mean density as a function of mass for different compositions. The red line corresponds to planets with purely rocky composition. The green line is for planets with 50% ice and 50% rocky composition. The blue line is for planet composed of pure ice. These three models are valid for low-mass planets with no significant envelope. The black curves corresponds to gas giant cores (figure from Mordasini et al. 2012).

Note that the mass-radius relationship changes during the evolution of a planetary system. At early stages planets are scattered more prominently as in the mass-radius plot shown in Figure 2.8. At late stages this scattering diminishes (see Figure 2.9)

and the relationship between mass and radius attains a shape of an elongated "S". The mass-radius relationship for the planets in the database is shown in Figure 2.10.

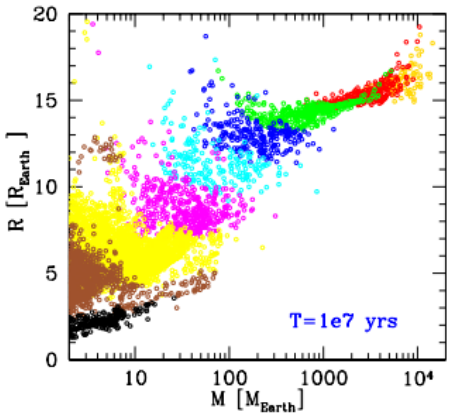

Figure 2.8: M-R relation at early stages of about 10 Myr (figure from Mordasini et al. 2012).

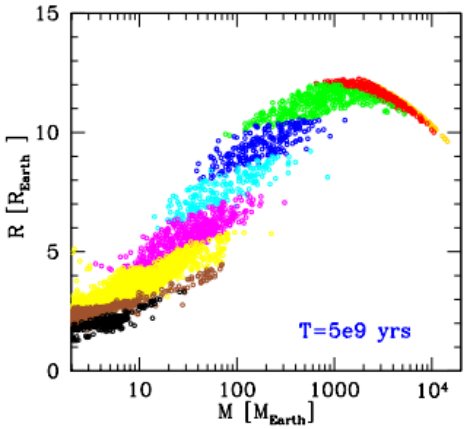

Figure 2.9: M-R relation at late stages of about 5 Gyr (figure from Mordasini et al. 2012).

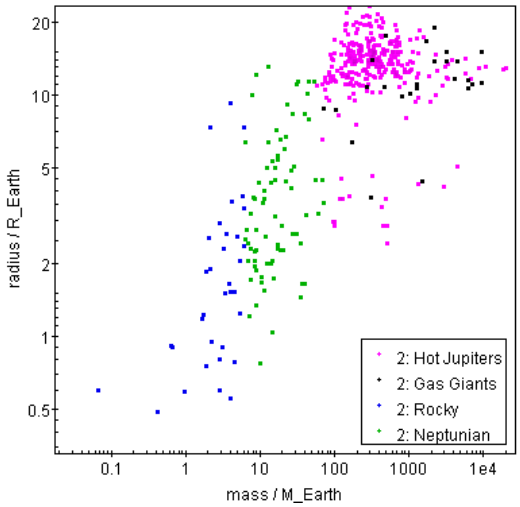

Figure 2.10: The correspondence between the mass and radius of all planets. The units are intentionally in Earth units to be able to compare this figure with Figure 2.9.

2.3 Database Reliability

We wanted to compare the densities of rocky and Neptunian planets against densities of all planets in the catalogue. By examining the density distribution of all planets one can see that some of them have extremely high densities, which is shown in Figure 2.11.

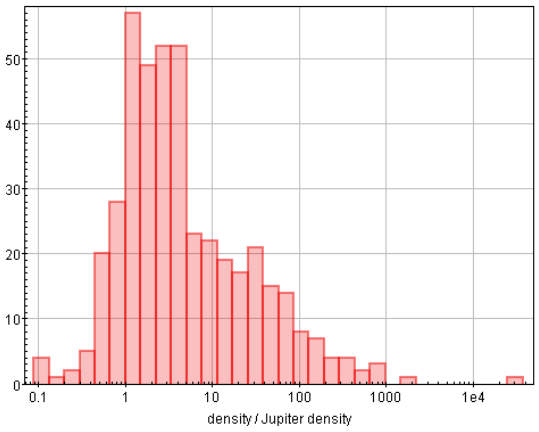

Figure 2.11: Density distribution of the exoplanets from the database.

Although most of the densities peak at reasonable values of order 1-4 Jupiter densities (this is also in a good agreement with the observational constraints) there are planets with densities up to 1000 Jupiter densities. The density of the Earth is $\sim$5.5 g/cm^3, which is similar to the density of other solar rocky planets. The gas giants are less dense: $\sim$1.3 g/cm^3 for Jupiter and Uranus, $\sim$0.69 g/cm^3 for Saturn and $\sim$1.6 g/cm^3 for Neptune (Allen & Cox 1999). A planet with a core composed by pure iron would have a density of 7.8 g/cm^3, which is less than twice the Earth density. In reality, the planetary core is exposed to the gravitational pressure induced by the overlying material. This "compressed rock" can reach higher densities: $\sim$13 g/cm^3 for the inner core of the Earth and a roughly estimated value of $\sim$25 g/cm^3 for the inner core of Jupiter.

The mean density of the planetary core in the right panel in Figure 2.7 varies over a wide range between 1 and 100 g/cm^3, which corresponds to $\sim$0.8-77 Jupiter densities. The density gradient flattens out at larger masses when electrons become degenerate and no further compression of the material can occur. Since the core of a gas giant is much denser than its outer regions, this shows once again that the high planetary densities as in Figure 2.11 are not possible to exist for real planets.

We also considered the fractional errors in mass and radius. As it is shown in the Figure 2.12, the fraction of error in the mass ranges between approximately 2-50%, while the error in the radius ranges with 2-20%. Although, the error in the radius is smaller than the error in the mass, we opted to base the definition of planetary types on mass because masses are available for more planets and the error is still small enough to not to affect the selection significantly.

Since the density distribution of the planets in the database gives incorrect results, it was interesting to compare its reliability with another database (at exoplanet.org).

New results for the density distribution were indeed different. Here, there were no extremely dense planets but, on the contrary, very loose (see Figure 2.13). These results are incorrect as well and do not give higher reliability.

In the case of the database at exoplanets.eu, the high densities are the likely result of very loose mass upper limits and/or errors in the mass of planets detected with the transit method. We neither changed the database nor did we check the density distribution for other available databases because it would be beyond the scope of this work.

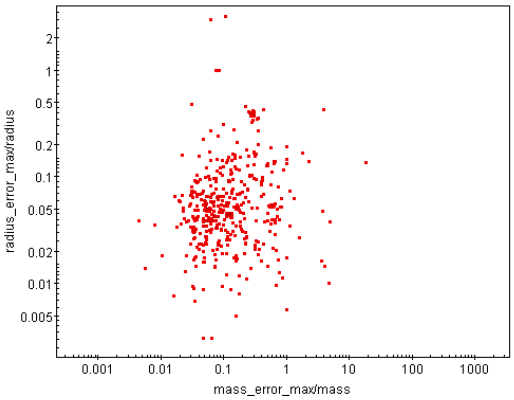

Figure 2.12: The fraction of error in mass and radius for the database at exoplanets.eu.

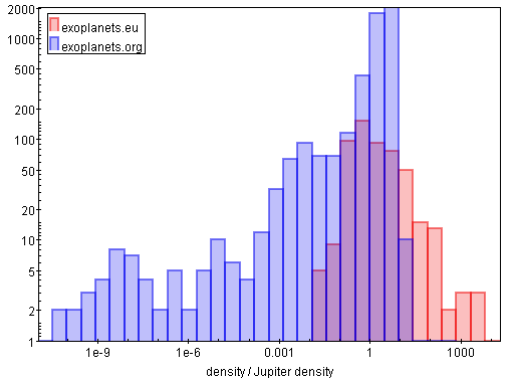

Figure 2.13: The density distribution of exoplanets in the database at exoplanets.eu (red) and exoplanets.org (blue).

2.4 Application of the Classification

When the classification of the planets was finished, we assigned a label to each planetary type for planets with both mass and semi-major axis. This procedure was performed in Matlab, where four planetary classes (hot Jupiters, gas giants, rocky and Neptunian planets) were defined and given a symbol (H, J, R, N respectively). We were also interested in the detection techniques and assigned a label for each detection technique as well. Radial velocity was denoted by R, primary transit by T, direct imaging by I, pulsar by P, astrometry by A, microlensing by M and other detection types by O.

All planets that belonged to the same star were grouped together. The result was a set of cell arrays, which contained the name of the star, a string with the symbols which denoted the planetary types and a second string with corresponding detection types. This procedure was performed separately for single- and multi-planetary systems. The obtained tables can be found in Appendix A.

These data were examined and some simple statistics were performed. First of all, the

systems with two planets were studied. There are 16 possible combinations of such systems. We were interested in whether all of them were present, if they were, how many there were and what detection techniques were used.

Another subject of our interest was systems with hot Jupiters and their migration. The configurations of multi-planetary systems with hot Jupiters were studied. Here we wanted to determine the number of systems with a hot Jupiter or hot Jupiters closest to the star, in between other planets and on the outskirts of the system. This might tell us whether other planets are ejected away from the system, while a gaseous giant migrates inwards.

We also examined the number of Earths and super-Earths detected by both transit and radial velocity techniques. Rocky and Neptunian planets in all systems detected by the transit were counted as well. These results were compared to the results found in published papers.

Moreover, we have defined the composition of a Solar System analogue depending on the used detection technique. The definition of the habitable zone was applied on the planets in the systems considered as Solar System analogues and studied further using available information in published papers.

Chapter 3

Results and Discussion

3.1 Planetary Systems

The study of two-planetary systems and their detection techniques has showed that some combinations of planets are more common than others. Systems with two gas giants (JJ) are the most abundant and are followed by other well-populated systems as Neptunian-Neptunian (NN), hot Jupiter-gas giant (HJ), Neptunian-gas giants (NJ) and hot Jupiter-hot Jupiter (HH) combinations in descending order. Detection of gas giants planets and Neptunes in wider orbits occurs by the Doppler technique. Hot Jupiters and other planets in close orbits tend to be detected by the transit.

Some other systems like hot Jupiter-rocky (HR), rocky-hot Jupiter (RH), hot Jupiter-Neptunian (HN), Neptunian-hot Jupiter (NH) and gas giant-rocky (JR) are not present at all. For the first four cases it might depend on migration of the hot Jupiter, which led to removal of other planets from the system. According to the present-day theories, migration of hot Jupiters can cause mean-motion resonances (MMR) with other planets, which gives them a kick in orbital period and eccentricity due to gravitational interactions. It may eventually lead to instability of the system and ejection of less massive planets (Raymond et al. 2008). An absence of gas giant-rocky systems might be a consequence of the limitations of the available detection instruments. Assuming that the gas giant in such a system was formed and remains beyond the snow line, the rocky planets must be at a very large distance from the host star, which is not preferable for either transit or Doppler techniques and lowers the chance of detecting the rocky planet.

These results are summarised in the Figure 3.1.

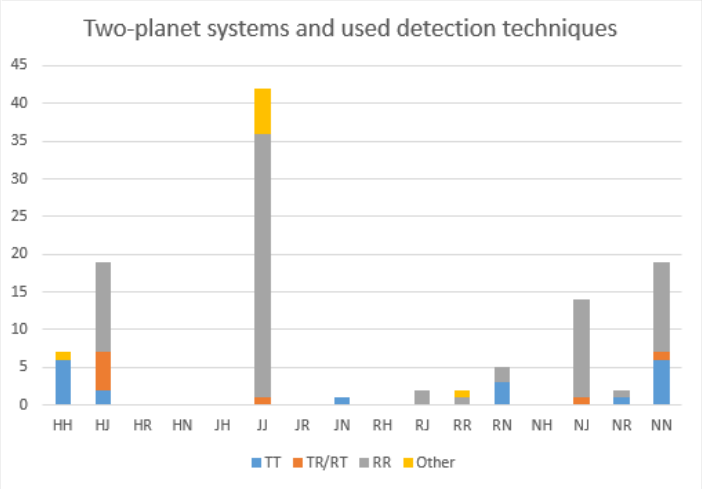

Figure 3.1: Two-planetary systems and techniques used to detect the planets. TT means that both planets were detected by the transit, RT/TR means that one of the planets was detected by the transit and the other one by the radial velocity and RR means that both planets were detected by the radial velocity.

Hot Jupiters

Presence and absence of hot Jupiters and their impact on the planetary systems were another interesting subjects to study. Table 3.1 shows the structure and number of systems with one or several hot Jupiters.

Table 3.1: Single- and multi-planetary systems with one or more hot Jupiters. Planets inside the squared brackets are optional. Three dots inside the squared brackets denote any possible planetary type of an optional planet. Note, that for multi-planetary systems, one letter does not necessarily mean one planet but can denote several planets of the same type following one after another.

Structure	Number of Systems
H	301
HH	7
HJ[R/N]	22
HR/N[J]	0
JH[R/N]	0
NH[...]	5
RH[...]	2

There is a relatively large number of multi-planetary systems containing a hot Jupiter and one or more gas giants (22 systems). We considered if it could depend on the separation between the clusters of gas giants and hot Jupiters. As it can be seen in

Figure 3.2, gas giant planets with semi-major axes of more than 10 AU pull the centroid of the gas giant cluster slightly to the right, which shifts the border between hot Jupiter and gas giant clusters. Thus, for a few planets, the k-means separation does not correlate with visual cluster separation and some gas giants with larger masses and slightly smaller orbits will be classified as hot Jupiters. Planets in hot Jupiter-gas giant(s) systems (HJ) are shown as yellow dots in Figure 3.2. Some planets do appear at the border between these two clusters, which means that classification of those planets may depend on the inclusion or exclusion of planets with semi-major axes larger than 10 AU. This means that some of hot Jupiter-gas giant(s) systems could be systems of two gas giants instead.

Nevertheless, most of the HJ couples do not lie on the cluster border and might be stable, probably due to a large orbital separation. However, it is rather impossible to find an explanation to this without running a simulation for these planetary systems. It is also evident that the gas giant tends to be more massive than the hot Jupiter. In Figure 3.3 hot Jupters and gas giants that belong to the same system are joint together by a black line showing this behaviour. The fact that hot Jupiters generally have lower masses than gas giants may depend on enhanced stellar irradiation at closer orbits, which leads to evaporation of the material from the surface of a planet and thus, a mass loss.

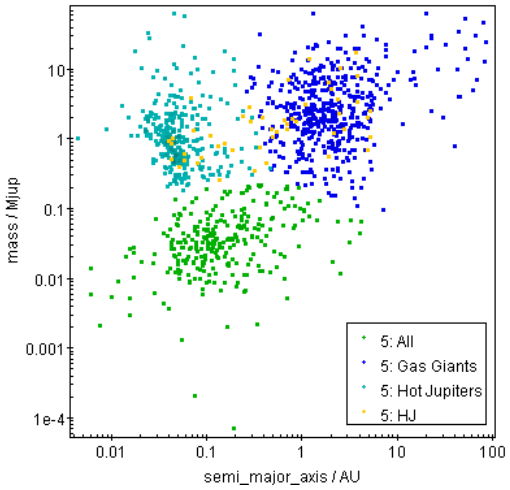

Figure 3.2: HJ couples (yellow dots) together with the rest of the planets distributed according to the semi-major axis and mass.

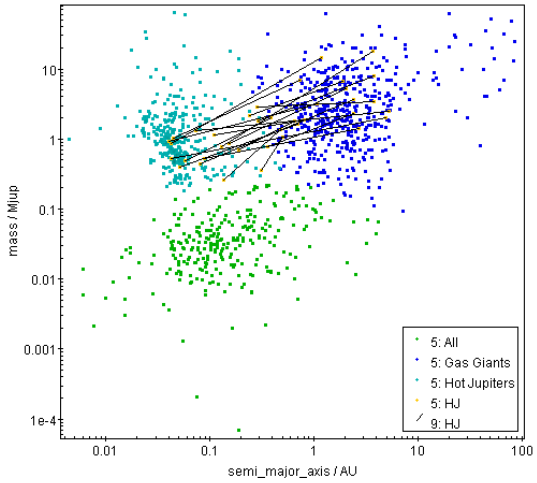

Figure 3.3: Same as in Figure 3.2. The black lines join hot Jupiters and gas giants that belong to the same system.

The systems, which have a Neptunian or a rocky planet closer to the host star than the hot Jupiter, have shown some interesting features. It is clear from the semi-major axis distributions shown in Figure 3.4 and 3.5 that some of the innermost rocky or Neptunian planets in these systems orbit their host stars at distances from where the innermost hot Jupiters from HH and HJ systems (Figure 3.4) and hot Jupiters from single-planetary systems (Figure 3.5) are. This suggests that hot Jupiters in R/NH[...] systems might still be migrating. A closer look at the periods of the planets in these systems reveals that some of the planets are almost in mean-motion resonance with the hot Jupiters (see Table 3.2). Thus, a reasonable conclusion is that these systems have not arrived at their final stage because a minor change in the semi-major axis of the hot Jupiters can lead to instability of a system and ejection of the less massive planets. However, MMR does not necessarily mean instability of a system and can also stabilise it.

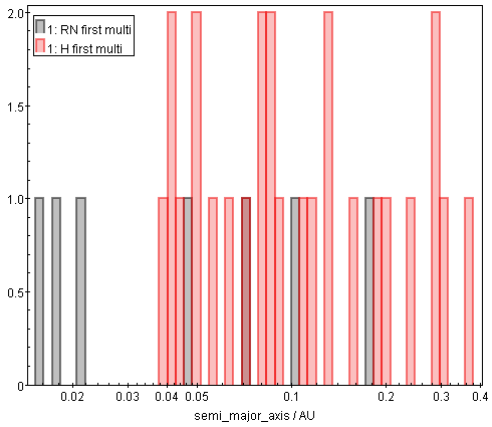

Figure 3.4: Semi-major axis distribution of the first planet in the multi-planetary systems, where the innermost planet is a rocky or Neptunian planet (gray) and a hot Jupiter (red) is present.

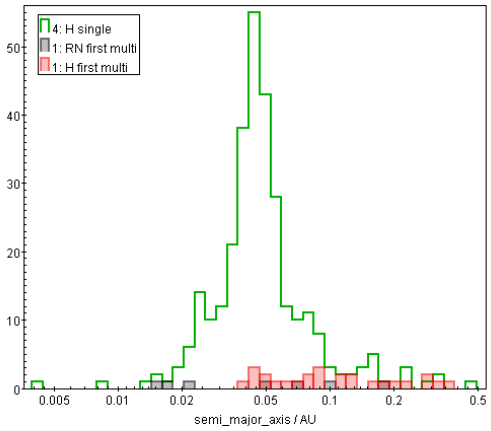

Figure 3.5: Same as in Figure 3.4, with also hot Jupiters in single-planetary systems (the green contour).

Table 3.2: Planetary systems, in which a hot Jupiter is near mean-motion resonance with another planet. a denotes semi-major axis, P_{p} is orbital period of a planet, $P_{\mathrm{min}}^{\mathrm{error}}$ and $P_{\mathrm{max}}^{\mathrm{error}}$ denote the minimum and maximum error in the orbital period respectively. The periods of the planets in near MMR are in bold type.

Planet	Planetary Type	a [AU]	P_{p} [days]	$P_{\mathrm{min}}^{\mathrm{error}}$ [days]	$P_{\mathrm{max}}^{\mathrm{error}}$ [days]
Kepler-30 b	N	0.18	**29.3**	0.008	0.008
Kepler-30 c	H	0.3	**60.3**	0.0002	0.0002
Kepler-30 d	N	0.5	143.3	0.009	0.009
Kepler-56 b	N	0.10	**10.5**	0.0011	0.0011
Kepler-56 c	H	0.16	**21.4**	0.00062	0.00062
Kepler-56 d	J	2	——	——	——
HIP 57274 b	N	0.07	**8.1**	0.004	0.004
HIP 57274 c	H	0.178	**32.0**	0.02	0.02
HIP 57274 d	J	1.01	431.7	8.5	8.5
HD 40307 b	R	0.048	**4.3**	0.00027	0.00027
HD 40307 c	H	0.081	**9.6**	0.0013	0.0013
HD 40307 d	N	0.13	20.4	0.0052	0.0052
HD 40307 e	R	0.19	34.6	0.21	0.21
HD 40307 f	R	0.25	51.56	0.14	0.14
HD 40307 g	N	0.6	197.8	5.7	9
Gliese 876 d	R	0.021	1.94	0.01	0.01
Gliese 876 c	H	0.13	**30.23**	0.19	0.19
Gliese 876 b	H	0.21	**61.03**	3.81	3.81
Gliese 876 e	N	0.33	124.69	90.04	90.04
WASP-47 e	N	0.017	0.79	$1.2 \cdot 10^{-5}$	$1.2 \cdot 10^{-5}$
WASP-47 b	H	0.051	**4.16**	$7.2 \cdot 10^{-5}$	$7.2 \cdot 10^{-5}$
WASP-47 d	N	0.088	**9.03**	0.00017	0.00017
WASP-47 c	J	1.36	572	7	7

Still, the number of systems with only one hot Jupiter is much larger than the number of multi-planetary systems containing one or more hot Jupiters, 301 against 36. This might be a matter of planetary formation in single-hot Jupiter systems or a result of planet-planet scattering meaning that systems with only one hot Jupiter are the most stable.

Earths and super-Earths

Martin & Livio (2015) quote results for the occurrence rate of rocky planets with masses in the range 1-10 $M_{\oplus}$, so called super-Earths, accounting for selection effects. The occurrence rate for super-Earths with a period $P_{\mathrm{p}}<50$ days detected by the Doppler technique is 10-20%. The occurrence rate of transiting planets is almost 50%, while for Kepler planets with radii $0.75<R_{\mathrm{p}}<2.5$ $R_{\oplus}$ and orbital periods of 50-300 days the

rate rises to 77% (Burke et al. 2015). Moreover, Fressin et al. (2013) present results for Earth-size planets with radii $0.8<R_p<1.25\ R_\oplus$ and orbital periods $P_p<85$ days. The occurrence rate for these planets is 18.4%.

In our case, different results are expected, mainly because we used a different definition for super-Earths. The mass of a super-Earth was allowed to vary in the range of 1-5.8 $M_\oplus$ [1], which decreased the number of super-Earth candidates compared to the definition above. We did not restrict the period either, however, the majority of the exoplanets had an orbital period $P_p<100$ days. Thus, according to Figure 1.2, the completeness values for super-Earths detected by the radial velocity and $P_p<100$ days decrease from ∼60% to ∼5% with larger orbital periods. For Earths the completeness decreases from ∼2% to 0%. According to Figure 1.5, the average completeness for Kepler super-Earths is 37% and 2.3% for Earths. Note, that these completeness values are currently the highest achieved for both transit and radial velocity techniques.

The results for the transit and radial velocity techniques are presented in Table 3.3. An absence of Earth-size planets detected by the Doppler technique is not surprising due to the small impact on the host star's radial velocity component. As it is predicted above, the transit technique managed to detect a small number of Earth-size planets. It is, however, obvious that the total amount of super-Earths detected by the transit is lower than by the radial velocity, which contradicts the predictions made above. This may a consequence of the completeness corrections of the occurrence rate for the planets done by the authors of the articles. Also, this could depend on the number of observed stars: if there were more stars observed by the radial velocity than by the transit, then there might be more Doppler planets because of this. Later in this section we describe more thoroughly how the correction of the occurrence rate affected the number of Neptunian and rocky planets detected by the transit.

Table 3.3: Extrasolar Earths and super-Earths detected by the transit and Doppler techniques in both single- and multi-planetary systems.

	Transit		Doppler	
	Multi-planetary	Single-planetary	Multi-planetary	Single-planetary
Super-Earths	21	4	32	4
Earths	2	1	0	0

[1] We decided not to change the mass limit of 5.8 $M_\oplus$ to 4 $M_\oplus$ as found in (Mordasini et al. 2012) because these values do not differ significantly. Also, the radius-mass relation in (Mordasini et al. 2012) depends on the composition of a planet, an unknown quantity in this case.

Neptunes and rocky planets detected by transit

Examination of the number of rocky and Neptunian planets in single- and multi-planetary systems has shown that extrasolar Neptunes are more abundant than Earths (see Table 3.4). However, it contradicts results presented by Petigura et al. (2013), who studied 129 Kepler planet candidates with radii less than 6 $R_\oplus$ and orbital periods 5-50 days. According to them, the occurrence of larger planets in their sample, i.e., Neptunian planets, is lower than of planets with radii of 1-2.8 $R_\oplus$. In order to understand the discrepancy between the results, we implemented the same restrictions as above and also recovered the planets in the database, which did not have any information about the semi-major axis and were therefore neglected before. Nevertheless, it did not lower the number of Neptunians or raise the number of rocky planets significantly. The answer to this lies in the correction for the completeness function of the occurrence rate, which was done by Petigura et al. 2013. Our data, on the other hand, were not corrected and thus, shows a lower number of small rocky planets than presented in the paper. The average completeness for planets with radii 1.0-1.41 $R_\oplus$ is 70%, while for planets with radii 1.41-2.0 $R_\oplus$ it is 89% (Petigura et al. 2013), which explains the decline in detected planets in our data (see Figure 3.6). Figure 3.7 shows that a plateau in the planet population below around 2.5 $R_\oplus$ is obtained due to corrections.

Table 3.4: Number of Neptunian and rocky planets detected by transit in single- and multi-planetary systems.

Transit			
Neptunes single	Neptunes multi	Rocky single	Rocky multi
17	56	5	26
73		31	

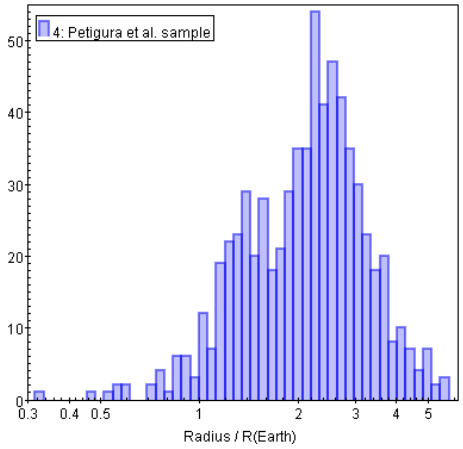

Figure 3.6: Radius distribution of planets in the sample with constrains from Petigura et al. (2013). A clear decrease in the number of detected planets with smaller radii is visible.

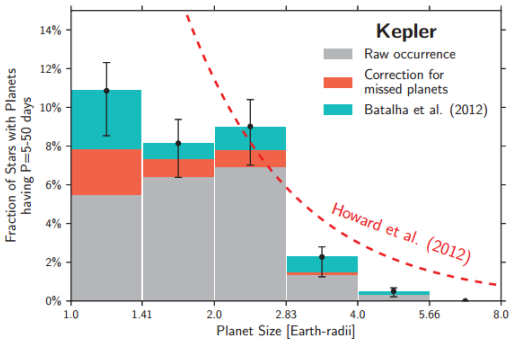

Figure 3.7: Radius distribution of Kepler planets presented by Petigura et al. (2013). Correction of the occurenence rate gives a plateau in the planet population at smaller radii (figure from Petigura et al. 2013).

3.2 Solar System Analogues

Selection bias of detection techniques substantially limit the possibility of finding Earth-size planets. Therefore, a broader definition for Solar System analogues (SSAs) is required.

Neptune and Uranus with their large orbital periods would most likely not be detected by current instruments. The same applies to the rocky planets due to their small sizes, although they orbit the Sun on relatively close orbits.

A SSA detected by the transit would probably look like a system with a super-Earth or a Neptunian planet in the innermost orbits and presumably a gas giant or a Neptunian further away on orbits corresponding to the orbit of Mars or less. Thus an expected composition of the system would be R/N[J/N], where planets inside the square brackets are optional.

A system observed by the Doppler technique would likely seem to consist of a gas giant at semi-major axes no larger than a few AU. The likelihood of detecting less massive planets is low even for short orbital periods. Then, a system would be expected to have a form of [R/N]J[N].

Planetary systems that were considered to be SSAs can be found in the Appendix B. The semi-major axis and mass distributions of the planets in these systems detected

by the transit and radial velocity are shown and compared to the Solar System planets in Figure 3.8 and 3.9 respectively. In agreement with selection effects, the planets tend to have shorter semi-major axes. Orbits of solar planets such as Saturn, Uranus and Neptune lie beyond the semi-major axis interval of detected planets in the solar-like systems.

The mass distribution of Doppler planets peaks at masses corresponding to super-Earths, while the mass of most of the transiting planets is spread out around Earth-like masses. Therefore, the biggest chance of detecting a low-mass rocky planet is if the planet is on a close orbit and is observed by the transit technique.

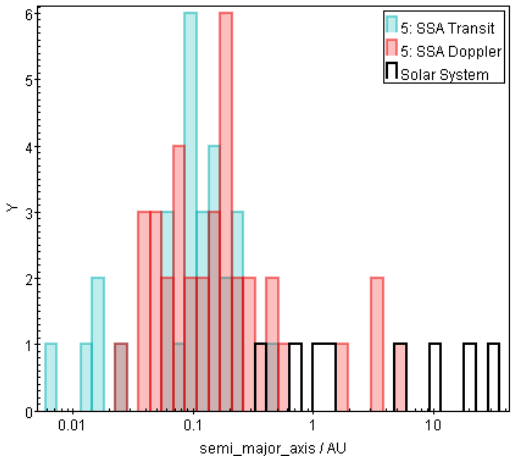

Figure 3.8: The distribution of the semi-major axis of planets in Solar-like systems. Transiting planets are marked with blue colour, magenta-coloured planets are detected by the Doppler technique and the black contour is for planets in the Solar System.

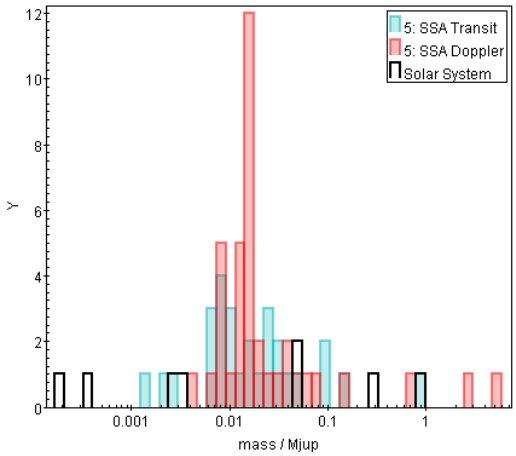

Figure 3.9: Mass distribution of the planets in Solar-like systems. The colouring is explaned in Figure 3.8.

Habitable Zone

Our definition of the HZ [2] gave seven candidates in six planetary systems that could harbour life. Six of these planets were super-Earths and only one Earth-like planet. Properties of these planets are shown in Table 3.5.

According to Anglada-Escudé et al. (2013) there are three habitable planets belonging to the GJ 667C system. The third candidate orbits the host star at a = 0.213 AU, which is beyond our definition of the HZ. However, a certain amount of a greenhouse

[2] See Section 1.3

gas, CO_2, is needed to be present in order to maintain the habitability of the planet.

The GI 581 c candidate was dismissed by Selsis et al. (2007), who argued that habitability of this planet is only possible if it is entirely cloud covered. As well as GJ 832 c, it is quite massive and might, thus, have a thick atmosphere, which increases the amount of greenhouse gases (Wittenmyer et al. 2014). Considering that both planets are close to the lower limit of the HZ, the greenhouse effect will contribute to higher surface temperature, undesirable for the maintenance of liquid water.

For Wolf 1061 c our results agree with Wright et al. (2016), who also find that this planet falls within the HZ of the host star.

Table 3.5: Rocky planets inside the HZ according to our definition and their properties. $P_{\rm p}$ denotes the orbital period of a planet, a is for semi-major axis, e means eccentricity, $T_*^{\rm eff}$ is stellar effective temperature, $HZ_{\rm min}$ and $HZ_{\rm max}$ mean the lower and upper limit for the HZ in a planetary system respectively.

Name	Mass [$M_\oplus$]	$P_{\rm p}$ [days]	a [AU]	e	$T_*^{\rm eff}$ [K]	$HZ_{\rm min}$ [AU]	$HZ_{\rm max}$ [AU]
GJ 667C c	3.8	28.14	0.125	0.02	3600.0	0.076	0.16
GJ 667C f	2.72	39.026	0.156	0.03	3600.0	0.076	0.16
GJ 682 b	4.42	17.478	0.08	0.08	3028.0	0.051	0.11
GJ 832 c	5.024	35.67	0.162	0.03	—	0.14	0.30
Gl 581 c	5.44	12.92	0.073	0.07	3498.0	0.067	0.14
Kepler-42 d	0.96	1.86	0.0154	—	3068.0	0.012	0.025
Wolf 1061 c	4.29	17.867	0.084	0.19	3393.0	0.044	0.094

The planets above orbit around cool stars: red and brown dwarfs. This means that the lower limit of the HZ is closer to the star compared to the Solar System. Planets orbiting their host stars at short distances are likely to be tidally locked [3] (Gillon et al. 2016). Hence, one hemisphere of a tidally locked planet always faces the host star (day side) and the other hemisphere is always dark (night side). Large temperature differences affect atmospheric circulations and set up conditions undesirable for life. Interestingly, there might be habitable regions on such planets in the regions between the day and night sides (Gillon et al. 2016). Also, Yang et al. (2014) has shown that slowly rotating planets can have the lower limit of the HZ at distances where they receive twice as high stellar flux as fast-rotating planets.

Moreover, chemical composition of the atmosphere (Wittenmyer et al. 2014) and the distribution of clouds has a major impact on the climate and habitability of a planet (Selsis et al. 2007). Loss of internal heat and magnetic field as in the case for Mars,

[3]Such planets have synchronised rotations with respect to their orbits due to tidal interactions with the host star (Gillon et al. 2016).

can transform a potentially habitable planet to uninhabitable.

Since many of these conditions are difficult to predict, the size of the HZ of a system becomes somewhat arbitrary. Furthermore, it changes during the lifetime of the host star as it evolves in the main sequence and its luminosity changes. Hence, a planet inside the HZ does not necessarily host life as well as a habitable planet does not have to be inhabited.

Chapter 4

Summary and Conclusions

The search of Solar System analogues requires a definition of different planetary types. By using a simple yet reliable k-means clustering algorithm in Matlab, the exoplanets from the database were easily divided into three clusters: one for gas giants, one for hot Jupiters, and one for rocky and Neptunians planets together.

We first tried to separate rocky from Neptunian planets according to their densities and, thus, besides the semi-major axis and mass, we also needed planets with measured radius. The result, however, was not satisfactory due to small number of data points, since only a fraction of the planets had measured radius and also due to errors in the parameters. In the second attempt, we used semi-major axis and mass and separated the planets by setting a mass limit of $\sim$5.8 $M_\oplus$. This mass limit was obtained by translating a published reference value for the maximum radius that a rocky planet can have (Wolfgang & Lopez 2015) and applying an average mass-radius relation.

We also studied selection effects of the transit and Doppler radial velocity techniques. Planets with large radii and short periods are most likely to be detected if observed by the transit, while massive short-period planets are more likely to be detected by the radial velocity technique. The distribution of planets in their classes showed to follow these expectations and selection effects.

When the exoplanets were classified we could examine obtained planetary systems. We then discovered that there is a large number of single-planetary systems containing a hot Jupiter. Multi-planetary systems with one or more hot Jupiters showed some interesting features. For instance, some of the hot Jupiters in these systems are almost in mean-motion resonance with other planets. This means that these systems may become unstable.

There is another type of planet not present in the Solar System, super-Earths, with masses in the range 1-5.8 $M_\oplus$ according to our definition. Due to larger radii and masses, super-Earths are more abundant in the catalogue than the Earth-like planets

since they are easier to detect. Kepler sample of super-Earths with periods of 50-200 days and radii $0.75<R<2.5\ R_{\oplus}$ shows an occurrence rate of 77% meaning that this type of planets is quite common, making the Solar System rare in this respect (Martin & Livio 2015).

We have also checked that the discrepancy between the number of transiting rocky and Neptunian planets in our database and the expected occurrence rate of those published by Petigura et al. (2013) is consistent with the magnitude of completeness corrections needed (our sample is not corrected).

Due to limitations of the present-day detection instruments, no strict analogues of the Solar System could be found. Small rocky planets and distant gas giants are difficult to detect. Nevertheless, the transit technique has managed to observe some low-mass rocky exoplanets on the innermost orbits. There are also some rocky planets lying in the so called habitable zone (HZ), which means that they might host life. However, this is a very complex matter and a planet inside the HZ does not necessarily harbour an alien life. A closer examination of planetary atmospheres, rotation and other factors must first be performed to conclude whether a planet is habitable or not.

The databases available today are far from complete and the question, whether there are any SSAs, remains unanswered. However, the ongoing research can give a deeper insight into this matter. One of the biggest latest announcements regards a discovery of more than 1200 verified Kepler planets [1]. It will undoubtedly help in the search of SSAs along with other anticipated exoplanet discoveries that might occur already in the foreseeable future.

Acknowledgements

I would like to extend my sincere gratitude to my supervisor Piero Ranalli for his excellent guidance and assistance. I am very thankful for his valuable advise, patience and ability to steer me in the right direction, which helped me in carrying out this project.

[1]The announcement can be found at `http://www.nasa.gov/press-release/nasas-kepler-mission-announces-largest-collection-of-planets-ever-discovered`

Bibliography

Allen, C. W. & Cox, A. N. 1999, Allen's Astrophysical quantities, 4th edn. (New York: AIP Press)

Anglada-Escudé, G., Tuomi, M., Gerlach, E., et al. 2013, A&A, 556, A126

Burke, C. J., Christiansen, J. L., Mullally, F., et al. 2015, ApJ The Astrophysical Journal, 809, 8

Chambers, J. 2010, Terrestrial Planet Formation, ed. S. Seager (University of Arizona Press)

Chambers, J. 2014, Icarus, 233, 83–100

D'Angelo, G., Durisen, R. H., & Lissauer, J. J. 2010, Giant Planet Formation, ed. S. Seager (University of Arizona Press)

Ford, E. B. 2014, Proceedings of the National Academy of Science, 111, 12616

Frank, J., King, A., & Raine, D. 2002

Fressin, F., Torres, G., Charbonneau, D., et al. 2013, ApJ The Astrophysical Journal, 766, 81

Gargaud, M., Amils, R., Quintanilla, J. C., et al. 2011, Encyclopedia of Astrobiology

Gillon, M., Jehin, E., Lederer, S. M., et al. 2016, Nature, 533, 221–224

Holman, M., Touma, J., & Tremaine, S. 1997, Nature, 386, 254

Ida, S. & Lin, D. N. C. 2004, ApJ, 616, 567

Kennedy, G. M. & Kenyon, S. J. 2008, ApJ, 673, 502

Kikuchi, A., Higuchi, A., & Ida, S. 2014, ApJ The Astrophysical Journal, 797, 1

Kitchin, C. R. 2012, Exoplanets: finding, exploring, and understanding alien worlds (Springer)

Kratter, K. M., Murray-Clay, R. A., & Youdin, A. N. 2010, ApJ, 710, 1375

Levison, H. F. & Agnor, C. 2003, Astron J The Astronomical Journal AJ, 125, 2692–2713

Lin, D. N. C. & Papaloizou, J. 1979, Monthly Notices of the Royal Astronomical Society, 186, 799–812

Lindegren, L. & Dravins, D. 2003, A&A, 401, 1185

Lissauer, J. J., Dawson, R. I., & Tremaine, S. 2014, Nature, 513, 336

Lubow, S. H. & Ida, S. 2010, Planet Migration, ed. S. Seager (University of Arizona Press)

Malmberg, D., Davies, M. B., & Heggie, D. C. 2011, MNRAS, 411, 859

Martin, R. G. & Livio, M. 2015, ApJ, 810, 105

Mayor, M., Lovis, C., & Santos, N. C. 2014, Nature, 513, 328

Mayor, M., Marmier, M., Lovis, C., et al. 2011, ArXiv e-prints

Molisch, A. F. & Oehry, B. P. 1998, Radiation trapping in atomic vapours (Clarendon Press)

Mordasini, C., Alibert, Y., Georgy, C., et al. 2012, A&A, 547, A112

Naoz, S., Farr, W. M., Lithwick, Y., Rasio, F. A., & Teyssandier, J. 2011, Nature, 473, 187

O'Brien, D. P., Morbidelli, A., & Levison, H. F. 2006, Icarus, 184, 39

Perryman, M. 2014, The Exoplanet Handbook

Petigura, E. A., Marcy, G. W., & Howard, A. W. 2013, ApJ, 770, 69

Pringle, J. E. 1981, Annual Review of Astronomy and Astrophysics Annu. Rev. Astro. Astrophys., 19, 137–160

Raymond, S. N., Barnes, R., Armitage, P. J., & Gorelick, N. 2008, ApJ, 687, L107

Raymond, S. N., Quinn, T., & Lunine, J. I. 2005, ApJ The Astrophysical Journal, 632, 670–676

Righter, K. & O'brien, D. P. 2011, Proceedings of the National Academy of Sciences, 108, 19165–19170

Schneider, J., Dedieu, C., Le Sidaner, P., Savalle, R., & Zolotukhin, I. 2011, A&A, 532, A79

Selsis, F., Kasting, J. F., Levrard, B., et al. 2007, A&A, 476, 1373

Silburt, A., Gaidos, E., & Wu, Y. 2015, ApJ, 799, 180

Taylor, M. B. 2005, in Astronomical Society of the Pacific Conference Series, Vol. 347, Astronomical Data Analysis Software and Systems XIV, ed. P. Shopbell, M. Britton, & R. Ebert, 29

Traub, W. A. & Oppenheimer, B. R. 2010, Direct Imaging of Exoplanets, ed. S. Seager (University of Arizona Press)

Winn, J. N. & Fabrycky, D. C. 2015, ARA&A, 53, 409

Wittenmyer, R. A., Tuomi, M., Butler, R. P., et al. 2014, ApJ, 791, 114

Wolfgang, A. & Lopez, E. 2015, ApJ, 806, 183

Wright, D. J., Wittenmyer, R. A., Tinney, C. G., Bentley, J. S., & Zhao, J. 2016, ApJ The Astrophysical Journal, 817

Yang, J., Boué, G., Fabrycky, D. C., & Abbot, D. S. 2014, ApJ The Astrophysical Journal, 787

Chapter 5

Appendix

Appendix A

Table 5.1: Single-planetary systems with determined planetary type and corresponding detection type.

Star Name	Planet	Detection Type
11 Com	J	R
11 UMi	J	R
14 And	J	R
14 Her	J	R
16 Cyg B	J	R
18 Del	J	R
1SWASP J1407	J	T
2M 1938+4603	J	P
2M 0103(AB)	J	I
2M 0122-2439	J	I
2M 044144	J	I
2M 0746+20	J	I
2M 2140+16	J	I
2M 2206-20	J	I
2M1207	J	I
30 Ari B	J	R
4 Uma	J	R
42 Dra	J	R
51 Eri	J	I
51 Peg	H	R
6 Lyn	J	R
7 CMa	J	R
70 Vir	J	R

continued Table 5.1

Star Name	Planet	Detection Type
75 Cet	J	R
8 Umi	J	R
81 Cet	J	R
91 Aqr	J	R
Aldebaran	J	R
BD +48 738	J	R
BD+15 2940	J	R
BD+20 274	J	R
BD+49 828	J	R
BD-10 3166	H	R
BD-114672	J	R
BD-17 63	J	R
BD14 4559	J	R
CD-35 2722	J	I
CFBDS 1458	J	I
CoRoT-1	H	T
CoRoT-10	H	T
CoRoT-11	H	T
CoRoT-12	H	T
CoRoT-13	H	T
CoRoT-14	H	T
CoRoT-15	H	T
CoRoT-16	H	T
CoRoT-17	H	T
CoRoT-18	H	T
CoRoT-19	H	T
CoRoT-2	H	T
CoRoT-20	H	T
CoRoT-21	H	T
CoRoT-22	N	T
CoRoT-23	H	T
CoRoT-25	H	T
CoRoT-26	H	T
CoRoT-27	H	T
CoRoT-28	H	T
CoRoT-29	H	T
CoRoT-3	H	T
CoRoT-33	H	T
CoRoT-4	H	T
CoRoT-5	H	T
CoRoT-6	H	T

continued Table 5.1

Star Name	Planet	Detection Type
CoRoT-8	H	T
CoRoT-9	J	T
DE0823-49	J	I
DP Leo	J	P
EPIC 201637175	H	T
GJ 1132	R	T
GJ 1214	N	T
GJ 160.2	N	R
GJ 176	N	R
GJ 229	N	R
GJ 27.1	N	R
GJ 3021	J	R
GJ 328	J	R
GJ 3341	H	R
GJ 3470	N	T
GJ 3634	N	R
GJ 422	N	R
GJ 436	N	T
GJ 504	J	I
GJ 674	N	R
GJ 758	J	I
GJ 849	J	R
Gl 15 A	R	R
Gl 179	J	R
Gl 687	N	R
Gl 785	N	R
Gl 86	H	R
HAT-P-1	H	T
HAT-P-11	N	T
HAT-P-12	H	T
HAT-P-14	H	T
HAT-P-15	H	T
HAT-P-16	H	T
HAT-P-18	H	T
HAT-P-19	H	T
HAT-P-2	H	T
HAT-P-20	H	T
HAT-P-21	H	T
HAT-P-22	H	T
HAT-P-23	H	T
HAT-P-24	H	T

continued Table 5.1

Star Name	Planet	Detection Type
HAT-P-25	H	T
HAT-P-26	N	T
HAT-P-27-WASP-40	H	T
HAT-P-28	H	T
HAT-P-29	H	T
HAT-P-3	H	T
HAT-P-30-WASP-51	H	T
HAT-P-31	H	T
HAT-P-32	H	T
HAT-P-33	H	T
HAT-P-34	H	T
HAT-P-35	H	T
HAT-P-36	H	T
HAT-P-37	H	T
HAT-P-38	H	T
HAT-P-39	H	T
HAT-P-4	H	T
HAT-P-40	H	T
HAT-P-41	H	T
HAT-P-42	H	T
HAT-P-43	H	T
HAT-P-45	H	T
HAT-P-49	H	T
HAT-P-5	H	T
HAT-P-50	H	T
HAT-P-51	H	T
HAT-P-52	H	T
HAT-P-53	H	T
HAT-P-54	H	T
HAT-P-55	H	T
HAT-P-56	H	T
HAT-P-57	H	T
HAT-P-6	H	T
HAT-P-7	H	T
HAT-P-8	H	T
HAT-P-9	H	T
HATS-1	H	T
HATS-10	H	T
HATS-13	H	T
HATS-14	H	T
HATS-2	H	T

continued Table 5.1

Star Name	Planet	Detection Type
HATS-3	H	T
HATS-4	H	T
HATS-5	H	T
HATS-6	H	T
HATS-8	N	T
HATS-9	H	T
HD 100655	J	R
HD 100777	J	R
HD 101930	H	R
HD 102117	N	R
HD 102195	H	R
HD 102329	J	R
HD 102365	N	R
HD 102956	H	R
HD 103197	N	R
HD 103720	H	R
HD 103774	H	R
HD 104067	N	R
HD 104985	J	R
HD 106252	J	R
HD 106270	J	R
HD 10647	J	R
HD 106515A	J	R
HD 10697	J	R
HD 107148	N	R
HD 108147	H	R
HD 108341	J	R
HD 108863	J	R
HD 109246	H	R
HD 109749	H	R
HD 110014	J	R
HD 111232	J	R
HD 113337	J	R
HD 114386	J	R
HD 114613	J	R
HD 114729	J	R
HD 114762	J	R
HD 114783	J	R
HD 116029	J	R
HD 117207	J	R
HD 11755	J	R

continued Table 5.1

Star Name	Planet	Detection Type
HD 118203	H	R
HD 11977	J	R
HD 120084	J	R
HD 121504	H	R
HD 122430	J	R
HD 125595	N	R
HD 12648	J	R
HD 126525	J	R
HD 126614	J	R
HD 129445	J	R
HD 130322	H	R
HD 131496	J	R
HD 13189	J	R
HD 132406	J	R
HD 132563B	J	R
HD 136418	J	R
HD 137388	J	R
HD 13931	J	R
HD 139357	J	R
HD 14067	J	R
HD 141937	J	R
HD 142022 A	J	R
HD 142245	J	R
HD 142415	J	R
HD 143361	J	R
HD 145377	J	R
HD 145457	J	R
HD 145934	J	R
HD 147513	J	R
HD 148156	J	R
HD 148427	J	R
HD 149026	H	T
HD 149143	H	R
HD 1502	J	R
HD 150433	J	R
HD 150706	J	R
HD 152079	J	R
HD 152581	J	R
HD 153950	J	R
HD 154088	R	R
HD 154345	J	R

continued Table 5.1

Star Name	Planet	Detection Type
HD 154672	J	R
HD 155233	J	R
HD 156279	J	R
HD 156411	J	R
HD 156668	R	R
HD 157172	N	R
HD 158038	J	R
HD 16141	N	R
HD 16175	J	R
HD 162004	J	R
HD 162020	H	R
HD 16417	N	R
HD 164509	J	R
HD 164595	N	R
HD 164604	J	R
HD 164922	J	R
HD 1666	J	R
HD 166724	J	R
HD 167042	J	R
HD 168746	H	R
HD 1690	J	R
HD 170469	J	R
HD 17092	J	R
HD 171028	J	R
HD 171238	J	R
HD 17156	H	T
HD 173416	J	R
HD 175167	J	R
HD 175541	J	R
HD 176051	J	A
HD 178911 B	J	R
HD 179079	N	R
HD 179949	H	R
HD 180314	J	R
HD 180902	J	R
HD 181342	J	R
HD 181720	J	R
HD 185269	H	R
HD 187085	J	R
HD 18742	J	R
HD 188015	J	R

continued Table 5.1

Star Name	Planet	Detection Type
HD 189567	N	R
HD 189733	H	T
HD 190647	J	R
HD 190984	J	R
HD 192263	H	R
HD 192310	N	R
HD 192699	J	R
HD 19467	J	I
HD 195019	H	R
HD 196050	J	R
HD 196067	J	R
HD 196885 A	J	R
HD 197037	J	R
HD 19994	J	R
HD 20367	J	R
HD 2039	J	R
HD 204941	J	R
HD 205739	J	R
HD 206610	J	R
HD 20782	J	R
HD 208487	J	R
HD 208527	J	R
HD 20868	J	R
HD 209458	H	T
HD 210277	J	R
HD 210702	J	R
HD 211847	J	R
HD 212301	H	R
HD 212771	J	R
HD 213240	J	R
HD 216435	J	R
HD 216437	J	R
HD 216536	J	R
HD 216770	J	R
HD 217786	J	R
HD 218566	N	R
HD 219077	J	R
HD 219415	J	R
HD 219828	N	R
HD 220074	J	R
HD 220689	J	R

continued Table 5.1

Star Name	Planet	Detection Type
HD 220773	J	R
HD 221287	J	R
HD 222155	J	R
HD 222582	J	R
HD 224693	H	R
HD 22781	J	R
HD 23079	J	R
HD 23127	J	R
HD 231701	J	R
HD 233604	J	R
HD 23596	J	R
HD 240210	J	R
HD 240237	J	R
HD 24040	J	R
HD 24064	J	R
HD 25171	J	R
HD 2638	H	R
HD 27442	J	R
HD 27631	J	R
HD 27894	H	R
HD 28185	J	R
HD 28254	J	R
HD 285507	H	R
HD 28678	J	R
HD 290327	J	R
HD 2952	J	R
HD 30177	J	R
HD 30562	J	R
HD 30669	J	R
HD 30856	J	R
HD 31253	J	R
HD 32518	J	R
HD 32963	J	R
HD 330075	H	R
HD 33142	J	R
HD 33283	H	R
HD 33564	J	R
HD 34445	J	R
HD 38283	J	R
HD 38801	J	R
HD 38858	N	R

continued Table 5.1

Star Name	Planet	Detection Type
HD 39091	J	R
HD 40979	J	R
HD 41004 A	J	R
HD 41004 B	H	R
HD 4113	J	R
HD 4203	J	R
HD 4208	J	R
HD 4308	N	R
HD 4313	J	R
HD 43197	J	R
HD 43691	H	R
HD 44219	J	R
HD 45184	N	R
HD 45350	J	R
HD 45652	H	R
HD 46375	H	R
HD 47536	J	R
HD 48265	J	R
HD 49674	N	R
HD 50499	J	R
HD 50554	J	R
HD 5319	J	R
HD 5608	J	R
HD 564	J	R
HD 5891	J	R
HD 59686	J	R
HD 62509	J	R
HD 63454	H	R
HD 63765	J	R
HD 6434	H	R
HD 66141	J	R
HD 66428	J	R
HD 6718	J	R
HD 68988	H	R
HD 70573	J	R
HD 70642	J	R
HD 7199	J	R
HD 72659	J	R
HD 73256	H	R
HD 73267	J	R
HD 73534	J	R

continued Table 5.1

Star Name	Planet	Detection Type
HD 75289	H	R
HD 75898	J	R
HD 76700	H	R
HD 77338	H	R
HD 79498	J	R
HD 80606	J	T
HD 81040	J	R
HD 81688	J	R
HD 82886	J	R
HD 83443	H	R
HD 8535	J	R
HD 85512	R	R
HD 8574	J	R
HD 86081	H	R
HD 86226	J	R
HD 86264	J	R
HD 8673	J	R
HD 87883	J	R
HD 88133	H	R
HD 89307	J	R
HD 90156	N	R
HD 93083	J	R
HD 95086	J	I
HD 95089	J	R
HD 95127	J	R
HD 95872	J	R
HD 96063	J	R
HD 96127	J	R
HD 96167	J	R
HD 97658	N	T
HD 98219	J	R
HD 98649	J	R
HD 99109	J	R
HD 99706	J	R
HD169142	J	I
HIP 105854	J	R
HIP 107773	J	R
HIP 116454	N	T
HIP 11915	J	R
HIP 12961	H	R
HIP 57050	H	R

continued Table 5.1

Star Name	Planet	Detection Type
HIP 63242	J	R
HIP 65891	J	R
HIP 70849	J	R
HIP 74865	J	I
HIP 75458	J	R
HIP 79431	J	R
HIP 91258	H	R
HIP 97233	J	R
HR 3549	J	I
HR 810	J	R
HU Aqr(AB)	J	P
HW Vir (AB)	J	P
KELT-1	H	T
KELT-10	H	T
KELT-15	H	T
KELT-2A	H	T
KELT-3	H	T
KELT-7	H	T
KELT-8	H	T
KIC 12557548	H	T
KIC 4862625(AB)	J	T
KMT-2015-1	J	M
KOI-1257 A	J	T
KOI-188	H	T
KOI-192	H	T
KOI-195	H	T
KOI-206	H	T
KOI-2939(AB)	J	T
KOI-314	R	T
KOI-372	J	T
KOI-680	H	T
KOI-830	H	T
Kepler-12	H	T
Kepler-15	H	T
Kepler-16 (AB)	J	T
Kepler-17	H	T
Kepler-19	N	T
Kepler-197	R	T
Kepler-21	N	T
Kepler-22	N	T
Kepler-31	J	T

continued Table 5.1

Star Name	Planet	Detection Type
Kepler-338	N	T
Kepler-34(AB)	J	T
Kepler-35(AB)	N	T
Kepler-38A	H	T
Kepler-39	H	T
Kepler-4	N	T
Kepler-40	H	T
Kepler-41	H	T
Kepler-412	H	T
Kepler-413 (AB)	N	T
Kepler-422	H	T
Kepler-423	H	T
Kepler-43	H	T
Kepler-44	H	T
Kepler-447	H	T
Kepler-45	H	T
Kepler-5	H	T
Kepler-6	H	T
Kepler-65	N	T
Kepler-66	H	T
Kepler-67	H	T
Kepler-7	H	T
Kepler-74	H	T
Kepler-75	H	T
Kepler-76	H	T
Kepler-77	H	T
Kepler-78	R	T
Kepler-8	H	T
Kepler-88	H	R
Kepler-91	H	T
Kepler-93	R	T
LKCA 15	J	I
MOA-2007-BLG-192-L	R	M
MOA-2007-BLG-197L	J	M
MOA-2007-BLG-400-L	J	M
MOA-2008-BLG-310-L	J	M
MOA-2008-BLG-379L	J	M
MOA-2009-BLG-266L	N	M
MOA-2009-BLG-319	J	M
MOA-2009-BLG-387L	J	M
MOA-2010-BLG-328L	N	M

continued Table 5.1

Star Name	Planet	Detection Type
MOA-2010-BLG-353L	J	M
MOA-2010-BLG-477L	J	M
MOA-2011-BLG-262L	N	M
MOA-2011-BLG-274	J	M
MOA-2011-BLG-293L	J	M
MOA-2011-BLG-322	J	M
MOA-2011-BLGL-028L	J	M
MOA-2013-BLG-220L	N	M
MOA-2013-BLG-605L	N	M
MOA-bin-1	J	M
NGC 2423 3	J	R
NGC 4349 No 127	J	R
NLTT 41135	H	T
OGLE-05-071L	J	M
OGLE-05-169L	N	M
OGLE-05-390L	R	M
OGLE-2007-BLG-368L	N	M
OGLE-2009-BLG-151_MOA-2009-232	J	M
OGLE-2011-BLG-0251	J	M
OGLE-2011-BLG-0265L	J	M
OGLE-2011-BLG-0420	H	M
OGLE-2012-BLG-0358L	J	M
OGLE-2012-BLG-0406L	J	M
OGLE-2012-BLG-0563L	J	M
OGLE-2013-BLG-0102L	J	M
OGLE-2013-BLG-0341L	R	M
OGLE-2013-BLG-0723LB	R	M
OGLE-2014-BLG-0124	J	M
OGLE-2015-BLG-0966	N	M
OGLE-TR-10	H	T
OGLE-TR-111	H	T
OGLE-TR-113	H	T
OGLE-TR-132	H	T
OGLE-TR-182	H	T
OGLE-TR-211	H	T
OGLE-TR-56	H	T
OGLE2-TR-L9	H	T
OGLE235-MOA53	J	M
OY Car	J	P
POTS-1	H	T
PSR 1719-14	H	P

continued Table 5.1

Star Name	Planet	Detection Type
PSR B1620-26	J	P
PZ Tel	J	I
Qatar-1	H	T
Qatar-2	H	T
RR Cae	J	P
SWEEPS-04	H	T
SWEEPS-11	H	T
TWA 5 A(AB)	J	I
TrES-1	H	T
TrES-2	H	T
TrES-3	H	T
TrES-4	H	T
TrES-5	H	T
UZ For(ab)	J	P
V391 Peg	J	P
WASP-1	H	T
WASP-10	H	T
WASP-100	H	T
WASP-101	H	T
WASP-103	H	T
WASP-104	H	T
WASP-106	H	T
WASP-108	H	T
WASP-109	H	T
WASP-11-HAT-P-10	H	T
WASP-110	H	T
WASP-111	H	T
WASP-112	H	T
WASP-117	H	T
WASP-12	H	T
WASP-120	H	T
WASP-121	H	T
WASP-122	H	T
WASP-123	H	T
WASP-13	H	T
WASP-135	H	T
WASP-14	H	T
WASP-15	H	T
WASP-16	H	T
WASP-17	H	T
WASP-18	H	T

continued Table 5.1

Star Name	Planet	Detection Type
WASP-19	H	T
WASP-2	H	T
WASP-20	H	T
WASP-21	H	T
WASP-22	H	T
WASP-23	H	T
WASP-24	H	T
WASP-25	H	T
WASP-26	H	T
WASP-28	H	T
WASP-29	H	T
WASP-3	H	T
WASP-31	H	T
WASP-32	H	T
WASP-33	H	T
WASP-34	H	T
WASP-35	H	T
WASP-36	H	T
WASP-37	H	T
WASP-38	H	T
WASP-39	H	T
WASP-4	H	T
WASP-42	H	T
WASP-43	H	T
WASP-44	H	T
WASP-45	H	T
WASP-46	H	T
WASP-48	H	T
WASP-49	H	T
WASP-5	H	T
WASP-50	H	T
WASP-52	H	T
WASP-55	H	T
WASP-58	H	T
WASP-6	H	T
WASP-61	H	T
WASP-62	H	T
WASP-63	H	T
WASP-65	H	T
WASP-66	H	T
WASP-67	H	T

continued Table 5.1

Star Name	Planet	Detection Type
WASP-68	H	T
WASP-69	H	T
WASP-7	H	T
WASP-70A	H	T
WASP-71	H	T
WASP-72	H	T
WASP-73	H	T
WASP-74	H	T
WASP-75	H	T
WASP-76	H	T
WASP-77A	H	T
WASP-78	H	T
WASP-79	H	T
WASP-8	H	T
WASP-80	H	T
WASP-82	H	T
WASP-83	H	T
WASP-84	H	T
WASP-85	H	T
WASP-87A	H	T
WASP-88	H	T
WASP-89	H	T
WASP-90	H	T
WASP-94 A	H	T
WASP-94 B	H	R
WASP-95	H	T
WASP-96	H	T
WASP-97	H	T
WASP-98	H	T
WASP-99	H	T
WISE 0458+6434 A	J	I
WISE 1217+16A	J	I
WISE 1711+3500	J	I
WISE J0720-0846	J	I
WTS-1	H	T
WTS-2	H	T
XO-1	H	T
XO-2N	H	T
XO-3	H	T
XO-4	H	T
XO-5	H	T

continued Table 5.1

Star Name	Planet	Detection Type
alf Ari	J	R
alf Cen B	R	R
beta Cnc	J	R
beta Pic	J	I
beta Umi	J	R
eps CrB	J	R
eps Eridani	J	R
eps Tau	J	R
gamma 1 Leo	J	R
gamma Cephei	J	R
kappa And	J	I
kappa CrB	J	R
ksi Aql	J	R
mu Leo	J	R
ome Ser	J	R
omi CrB	J	R
omi UMa	J	R
sig Per	J	R
tau Boo	H	R
tau Gem	J	R

Table 5.2: Multi-planetary systems with determined planetary types and corresponding detection types.

Star Name	Planets	Detection Types
Kepler-24	HH	TT
Kepler-26	HH	TT
Kepler-27	HH	TT
Kepler-28	HH	TT
Kepler-29	HH	TT
Kepler-32	HH	TT
Kepler-46	HH	TO
HAT-P-13	HJ	TR
HAT-P-17	HJ	TR
HAT-P-44	HJ	TT
HAT-P-46	HJ	TT
HD 13908	HJ	RR
HD 147018	HJ	RR
HD 159243	HJ	RR
HD 163607	HJ	RR
HD 187123	HJ	RR
HD 217107	HJ	RR
HD 37605	HJ	RR
HD 38529	HJ	RR
HD 52265	HJ	RR
HD 74156	HJ	RR
HD 9446	HJ	RR
KELT-6	HJ	TR
Kepler-424	HJ	TR
WASP-41	HJ	TR
XO-2S	HJ	RR
HIP 14810	HJJ	RRR
HD 141399	HJJJ	RRRR
ups And	HJJJ	RRRR
24 Sex	JJ	RR
BD20 2457	JJ	RR
GJ 317	JJ	RR
HD 102272	JJ	RR
HD 108874	JJ	RR
HD 113538	JJ	RR
HD 11506	JJ	RR
HD 12661	JJ	RR
HD 128311	JJ	RR

continued Table 5.2

Star Name	Planets	Detection Types
HD 134987	JJ	RR
HD 142	JJ	RR
HD 154857	JJ	RR
HD 155358	JJ	RR
HD 159868	JJ	RR
HD 1605	JJ	RR
HD 168443	JJ	RR
HD 169830	JJ	RR
HD 183263	JJ	RR
HD 200964	JJ	RR
HD 202206	JJ	RR
HD 207832	JJ	RR
HD 33844	JJ	RR
HD 47366	JJ	RR
HD 60532	JJ	RR
HD 67087	JJ	RR
HD 73526	JJ	RR
HD 7449	JJ	RR
HD 89744	JJ	RR
HD 92788	JJ	RR
HIP 5158	JJ	RR
HIP 67851	JJ	RR
HIP 73990	JJ	II
HR 228	JJ	RR
KOI-1474	JJ	TO
Kepler-432	JJ	TR
NN Ser (ab)	JJ	PP
NY Vir	JJ	PP
OGLE-06-109L	JJ	MM
OGLE-2012-BLG-0026L	JJ	MM
TYC+1422-614-1	JJ	RR
eta Cet	JJ	RR
nu Oph	JJ	RR
47 Uma	JJJ	RRR
HD 37124	JJJ	RRR
HD 82943	JJJ	RRR
HR 8799	JJJJ	IIII
KOI-1574	JN	TT
HIP 57274	NHJ	RRR
Kepler-56	NHJ	TTR
Kepler-30	NHN	TTT

continued Table 5.2

Star Name	Planets	Detection Types
WASP-47	NHNJ	OTOR
55 Cnc	NHNNJ	TRRRR
BD-082823	NJ	RR
Gl 649	NJ	RR
HD 11964	NJ	RR
HD 134060	NJ	RR
HD 177830	NJ	RR
HD 190360	NJ	RR
HD 215456	NJ	RR
HD 215497	NJ	RR
HD 45364	NJ	RR
HD 47186	NJ	RR
HD 65216	NJ	RR
HD 85390	NJ	RR
HD 99492	NJ	RR
Kepler-454	NJ	TR
HD 125612	NJJ	RRR
HD 181433	NJJ	RRR
HD 204313	NJJ	RRR
mu Ara	NJJJ	RRRR
CoRoT-7	NN	TR
EPIC 203771098	NN	TT
GJ 180	NN	RR
GJ 3293	NN	RR
HD 109271	NN	RR
HD 117618	NN	RR
HD 13808	NN	RR
HD 20003	NN	RR
HD 20781	NN	RR
HD 21693	NN	RR
HD 3651	NN	RR
HD 51608	NN	RR
HD 93385	NN	RR
HD 96700	NN	RR
K2-19	NN	TT
Kepler-25	NN	TT
Kepler-279	NN	TT
Kepler-396	NN	TT
Kepler-85	NN	TT
BD-061339	NNN	RRR
Gl 163	NNN	RRR

continued Table 5.2

Star Name	Planets	Detection Types
HD 134606	NNN	RRR
HD 31527	NNN	RRR
HD 69830	NNN	RRR
HD 7924	NNN	RRR
Kepler-18	NNN	TTT
Kepler-23	NNN	TTT
KOI-94	NNNN	TTTT
HD 10180	NNNNNJ	RRRRRR
Kepler-114	NNR	TTT
HD 1461	NR	RR
Kepler-305	NR	TT
K2-3	NRN	TTT
Kepler-20	NRNNN	TTTTT
Kepler-62	NRNNN	TTTTT
Kepler-79	NNNR	TTTT
Gliese 876	RHHN	RRRR
HD 40307	RHNRRN	RRRRRR
GJ 433	RJ	RR
GJ 832	RJ	RR
CoRoT-24	RN	TT
GJ 682	RN	RR
Kapteyn's	RN	RR
Kepler-10	RN	TT
Kepler-36	RN	TT
GJ 676A	RNJJ	RRRR
61 Vir	RNN	RRR
HD 136352	RNN	RRR
Kepler-37	RNN	TTT
Kepler-9	RNN	TTT
Gl 581	RNR	RRR
Kepler-60	RNR	TTT
HD 215152	RR	RR
KOI-55	RR	II
Kepler-68	NRJ	TTR
Kepler-51	RRN	TTO
HD 219134	RRNNNRJ	TRRRRRR
Kepler-11	RRNNRJ	TTTTTT
Kepler-102	RRNR	TTTT
HD 20794	RRR	RRR
HD 39194	RRR	RRR
Kepler-42	RRR	TTT

continued Table 5.2

Star Name	Planets	Detection Types
PSR 1257 12	RRR	PPP
Wolf 1061	RRR	RRR
GJ 667C	RRRRRR	RRRRRR

Appendix B

Table 5.3: Planetary systems considered as Solar System analogues.

Star Name	Planetary Types	Detection Types
Kepler-114	NNR	TTT
HD 1461	NR	RR
Kepler-305	NR	TT
K2-3	NRN	TTT
Kepler-20	NRNNN	TTTTT
Kepler-62	NRNNN	TTTTT
GJ 433	RJ	RR
GJ 832	RJ	RR
CoRoT-24	RN	TT
GJ 682	RN	RR
Kapteyn's	RN	RR
Kepler-10	RN	TT
Kepler-36	RN	TT
GJ 676A	RNJJ	RRRR
61 Vir	RNN	RRR
HD 136352	RNN	RRR
Kepler-37	RNN	TTT
Kepler-9	RNN	TTT
Gl 581	RNR	RRR
Kepler-60	RNR	TTT
HD 215152	RR	RR
Kepler-68	NRJ	TTR
HD 219134	RRNNNRJ	TRRRRRR
Kepler-11	RRNNRJ	TTTTTT
Kepler-102	RRNR	TTTT
HD 20794	RRR	RRR
HD 39194	RRR	RRR
Kepler-42	RRR	TTT
Wolf 1061	RRR	RRR
GJ 667C	RRRRRR	RRRRRR